Review of Applied Science and Technology

Volume: 3; **Issue:** 2
Pages: 92– 140

open access
Crossref

Machine Learning Enhanced GIS And AHP Modeling for High-Resolution Flood-Susceptibility Prediction, Vulnerability Assessment, and Risk Classification

Md Kaium Hossain[1];

[1]. *Graduate Assistant, Western Illinois University GIS Centre, Illinois, USA;*
Master of Science in GIScience and Geoenvironment; Western Illinois University, Illinois, USA;
Email: k-hossain@wiu.edu; kaiumhossain37@gmail.com;

Doi: 10.63125/fz8hv245
Received: 11 March 2024; **Revised:** 14 April 2024; **Accepted:** 13 May 2024; **Published:** 07 June 2024

Abstract

Flood-risk management often relies on generalized hazard maps that inadequately represent localized interactions among hydrological conditions, environmental characteristics, exposure, and multidimensional vulnerability, thereby limiting the accuracy and practical value of risk classification. This study aimed to develop and evaluate an integrated machine learning enhanced Geographic Information System and Analytic Hierarchy Process framework for high-resolution flood-susceptibility prediction, vulnerability assessment, and risk classification within a selected flood-prone case-study area. A quantitative, cross-sectional, explanatory, predictive, and case-based design was employed, combining structured stakeholder assessment with spatial modelling. From 340 distributed questionnaires, 312 were returned and 300 valid responses were retained from GIS specialists, hydrologists, disaster-management professionals, environmental officers, engineers, urban planners, government officials, researchers, emergency personnel, and community representatives. The principal variables included geospatial and hydrological data quality, AHP weighting effectiveness, machine-learning predictive capability, GIS-AHP-ML integration capability, socioeconomic and demographic vulnerability, physical, environmental, and infrastructural vulnerability, flood-susceptibility prediction effectiveness, vulnerability-assessment effectiveness, and integrated flood-risk classification effectiveness. Data were analyzed using descriptive statistics, reliability and validity testing, Pearson correlation, multiple regression, ANOVA, AHP consistency analysis, and comparative machine-learning evaluation. The instrument showed strong reliability, with Cronbach's alpha values from .821 to .914, while KMO reached .891. Random Forest achieved the strongest predictive performance, with 88.7% accuracy, 89.4% recall, an F1-score of 88.6%, and an AUC of .931. High and very high susceptibility zones covered 37.2% of the study area but contained 70.1% of observed flood locations. High and very high-risk zones represented 39.4% of the area, 57.6% of the exposed population, and 60.2% of exposed infrastructure. The three regression models explained 68.2%, 59.7%, and 64.9% of the variance in susceptibility prediction, vulnerability assessment, and risk classification, respectively. The findings imply that accurate spatial data, transparent expert weighting, validated machine-learning models, and multidimensional vulnerability indicators should be integrated to improve flood planning, infrastructure protection, preparedness, and resource prioritization.

KEYWORDS
Machine Learning; Geographic Information System; Analytic Hierarchy Process; Flood-Susceptibility Prediction; Flood-Risk Classification

INTRODUCTION

Flooding refers to the temporary inundation of land that is normally dry when river discharge, intense precipitation, surface runoff, coastal water, drainage congestion, or hydrological overflow exceeds the capacity of natural and constructed drainage systems. In flood-related research, hazard refers to the physical occurrence, magnitude, frequency, and spatial extent of inundation, while susceptibility describes the relative tendency of a geographical location to experience flooding based on its environmental, topographical, hydrological, and land-use characteristics. Exposure represents the presence of people, settlements, infrastructure, agricultural land, economic assets, and public services within areas that may be affected by flooding. Vulnerability refers to the degree to which exposed populations, physical structures, economic systems, infrastructure, and environmental resources are likely to experience damage or disruption. Flood risk consequently represents the combined interaction among flood hazard or susceptibility, exposure, and vulnerability. These concepts must be distinguished because a location may demonstrate high flood susceptibility but relatively low risk when population and infrastructure exposure are limited. Conversely, an area with moderate flood susceptibility may experience severe risk when it contains dense settlements, fragile infrastructure, economically disadvantaged households, or limited emergency-response capacity. Flooding has substantial international significance because it affects both developed and developing countries and causes extensive mortality, displacement, infrastructure failure, agricultural loss, environmental degradation, business interruption, and economic damage. Satellite-based examination of 913 major flood events occurring between 2000 and 2018 identified approximately 2.23 million square kilometres of inundated land and estimated that between 255 million and 290 million people were directly affected by flooding during that period (Tellman et al., 2021). A high-resolution global flood assessment further estimated that approximately 1.81 billion people, representing nearly 23 percent of the global population, were directly exposed to flood depths exceeding 0.15 metres under a 1-in-100-year flood scenario (Rentschler et al., 2022). Large proportions of this exposure were concentrated in South Asia, East Asia, and lower-income countries where rapid urbanization, population concentration, weak drainage systems, and limited adaptive resources frequently intensify flood consequences. Global research has also demonstrated that riverine and coastal flood zones contain considerable concentrations of population and economic activity (Jongman et al., 2012). International flood-risk frameworks have therefore emphasized the need to integrate hydrological hazard information with population distribution, land use, infrastructure, and economic data at compatible spatial resolutions (Winsemius et al., 2013). European flood-mapping practices have similarly demonstrated that flood extent and depth maps are more widely available than comprehensive risk maps that incorporate the consequences of flooding for society and the economy (Moel et al., 2009). Economic flood-damage assessment has further established that credible flood-risk analysis requires careful consideration of direct and indirect losses, spatial boundaries, vulnerability functions, model assumptions, and validation procedures rather than relying exclusively on inundation extent or depth (Merz et al., 2010). Geographic Information Systems constitute a spatially organized technological framework through which flood-related environmental, hydrological, topographical, social, and infrastructural datasets can be collected, standardized, processed, analysed, overlaid, modelled, and visualized. GIS-based flood-susceptibility analysis transforms multiple geographical variables into georeferenced raster or vector layers and evaluates the relative susceptibility of each spatial unit according to the factors associated with previous or potential flood occurrence. Frequently used flood-conditioning factors include elevation, slope, aspect, curvature, rainfall intensity, flow accumulation, drainage density, distance from rivers, land use and land cover, soil characteristics, lithology, topographic wetness index, stream power index, normalized difference vegetation index, road density, building density, and impervious surface coverage. Each factor represents a particular mechanism that may influence runoff production, infiltration, water concentration, drainage connectivity, overland flow, and the capacity of a landscape to retain or transmit water. Elevation and slope influence the direction and speed of surface runoff, while drainage density and distance from rivers affect hydrological connectivity and proximity to potential overflow. Land-use change, vegetation removal, urban development, road construction, and surface sealing can reduce infiltration and increase runoff accumulation. The analytical contribution of GIS is therefore broader than the production of flood maps because GIS provides the spatial environment required to harmonize satellite images, digital elevation models, rainfall records, soil maps, hydrographic networks, administrative boundaries, infrastructure datasets, and historical flood inventories. Regional flood-hazard analysis in Greece used flow accumulation, distance from drainage networks, elevation, land use, rainfall intensity, geology, and slope to construct and validate a flood-hazard index against historical flood records (Kazakis et al., 2015). National-scale flood-susceptibility analysis in Slovakia used hydrographic, hydrological, morphometric, and permeability-related variables within a 50-metre raster environment and found considerable agreement between historically recorded flood locations and areas classified as highly susceptible (Vojtek & Vojteková, 2019). These findings demonstrate that flood susceptibility is not observed as a single measurable condition but is generated through the spatial interaction of numerous conditioning factors. Spatial resolution is particularly important because coarse-resolution datasets can conceal localized terrain depressions, drainage obstructions, riverbank variations, road embankments, small channels, and urban runoff pathways. Changes in digital elevation model resolution have been found to influence both the predictive accuracy of machine-learning flood models and the representation of terrain-derived variables (Avand et al., 2022). The resolution of elevation data also affects the calculation of the topographic wetness index and its contributing-area and slope components (Sørensen & Seibert, 2007). High-resolution flood-susceptibility prediction must therefore preserve local spatial heterogeneity, maintain alignment among raster layers, accurately represent terrain and drainage conditions, and validate predictions at a spatial scale appropriate to the selected case-study area.

Figure 1: Integrated research design for GIS, AHP, and machine learning-based flood risk assessment

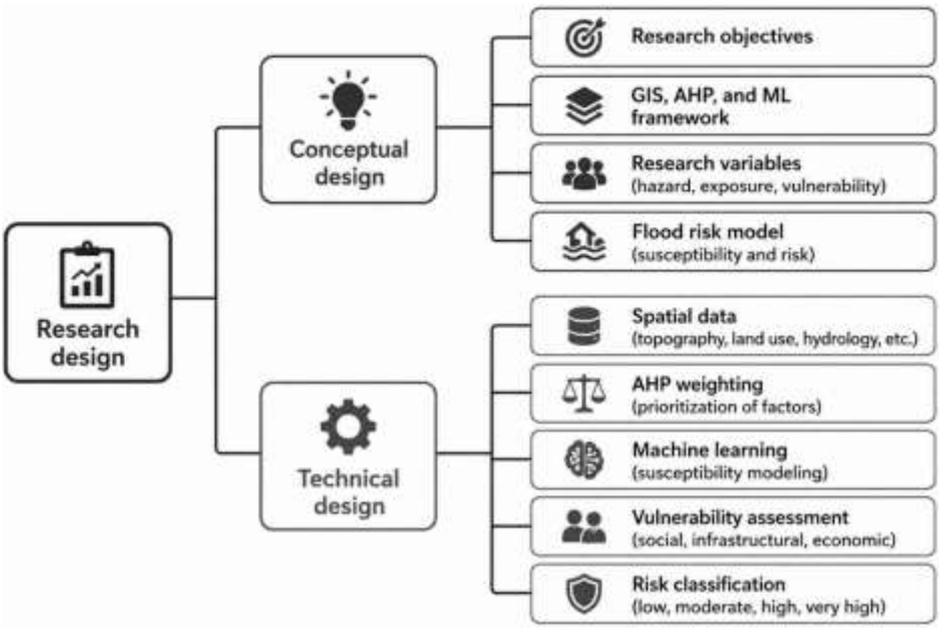

The Analytic Hierarchy Process is a structured multi-criteria decision-analysis method that divides a complex problem into a hierarchy consisting of an overall objective, decision criteria, subcriteria, and alternatives. Within flood-susceptibility assessment, AHP converts expert knowledge concerning the relative importance of flood-conditioning variables into numerical weights that can be integrated with standardized GIS layers. Experts compare each criterion with every other criterion using an ordered preference scale, and the resulting pairwise comparison matrix is normalized to calculate a priority vector representing the relative contribution of each factor. The consistency of the expert judgments is evaluated through the Consistency Index and Consistency Ratio. A Consistency Ratio below 0.10 is commonly regarded as evidence that the pairwise comparisons are acceptably coherent. Following the determination of criteria weights, the standardized spatial layers are multiplied by their respective weights and combined through weighted linear combination or weighted overlay analysis. The resulting continuous index is subsequently classified into ordered flood-susceptibility categories such as very low, low, moderate, high, and very high. AHP-based flood studies have demonstrated that susceptibility is influenced by both natural watershed characteristics and anthropogenic modifications. Analysis of flood hazard using natural and human-related factors found that stream-channel modification, watershed alteration, and other human interventions can increase flood hazard independently of natural basin conditions (Stefanidis & Stathis, 2013). An integrated urban flood study in Kenya combined rainfall, elevation, slope, drainage, land use, and soil variables through GIS and AHP to produce flood-vulnerability and risk maps at the municipal level (Ouma & Tateishi, 2014). Multi-criteria flood-prone-area mapping has also combined hydrological, geomorphological, and land-cover indicators to identify potential flood locations under conditions of limited observational data (Papaioannou et al., 2015). A regional flood-hazard framework using seven flood-related parameters applied AHP-generated weights and sensitivity analysis to evaluate the stability of the resulting susceptibility classes (Kazakis et al., 2015). Methodological variations have been introduced to address the uncertainty involved in expert comparisons. Conventional AHP, fuzzy AHP, and interval rough AHP have been compared in urban flood-hazard mapping, showing that uncertainty-sensitive weighting methods can alter both the spatial distribution and validation performance of flood classes (Gigović et al., 2017). Spatial sensitivity analysis has further demonstrated that relatively small changes in criteria weights may produce local changes in vulnerability classifications (Feizizadeh & Kienberger, 2017). Spatially explicit uncertainty analysis has similarly identified geographical areas in which flood-vulnerability categories are less stable because of the influence of particular criteria and their spatial distributions (Brito et al., 2019). AHP therefore provides a transparent and systematic basis for ranking flood-conditioning factors, although the quality of its outputs depends on expert selection, judgment consistency, factor classification, spatial resolution, and the assumption that weighted additive relationships sufficiently represent complex flood processes.

Machine learning refers to a group of computational approaches that identify patterns, associations, and predictive relationships within data and apply those learned relationships to classify new observations or estimate unknown outcomes. In flood-susceptibility modelling, supervised machine-learning algorithms are trained using historical flood and non-flood locations together with corresponding values for environmental and hydrological conditioning factors. Once trained, the models are applied to all spatial units within the study area to estimate flood probability or classify the landscape according to different levels of susceptibility. Commonly used algorithms include logistic regression, support vector machines, decision trees, random forests, artificial neural networks, naïve Bayes trees, adaptive neuro-fuzzy inference systems, gradient-boosting methods, XGBoost, deep-belief networks, and long short-term memory networks. These algorithms are particularly relevant to flood prediction because the relationships among rainfall, terrain, drainage, land use, soil, vegetation, and proximity variables are often nonlinear, interactive, and spatially heterogeneous. A GIS-based support vector machine assessment demonstrated that kernel selection influenced predictive accuracy and that radial-basis and linear kernels performed more strongly than a frequency-ratio benchmark in the examined watershed (Mansor, et al., 2015). The integration of support vector machines with frequency-ratio information also showed that combining statistical evidence with machine-learning classification can improve flood-susceptibility modelling (Pradhan, & Jebur, 2015). Comparative analysis of alternating decision trees, naïve Bayes trees, logistic model trees, and reduced-error pruning trees found substantial differences in predictive performance even when the models used the same flood inventory and conditioning-factor dataset (Khosravi et al., 2018). Hybrid adaptive neuro-fuzzy inference systems optimized with genetic algorithms and differential evolution techniques have also produced high-performing susceptibility maps (Hong et al., 2018). Similar modelling has combined adaptive neuro-fuzzy inference systems with biogeography-based optimization and bat algorithms to improve calibration and classification accuracy (Ahmadlou et al., 2019). Comparisons among random forest, naïve Bayes tree, and alternating decision tree methods found that random forest achieved the strongest overall performance for the examined dataset (Chen et al., 2020). Ensemble approaches combining evidential belief functions and binomial logistic regression have also been used to model flood susceptibility in river basins in eastern India (Chowdhuri et al., 2020). Advanced ensemble models involving Dagging, random subspace, artificial neural networks, random forest, and support vector machines have produced area-under-the-curve values exceeding 0.80 in Bangladesh and have revealed meaningful performance differences among algorithms (Islam et al., 2021). Long short-term memory networks have been applied to learn spatial dependencies among flood-related conditioning variables (Fang et al., 2021), while deep-belief networks optimized through backpropagation and genetic algorithms have generated high validation accuracy in flash-flood susceptibility modelling (Shahabi et al., 2021). The effectiveness of machine learning therefore depends on the quality of the flood inventory, predictor selection, model calibration, validation design, class balance, spatial resolution, and performance-evaluation procedures (Mosavi et al., 2018).

An integrated GIS, AHP, and machine-learning framework conceptualizes flood susceptibility as both a spatial multi-criteria decision problem and a data-driven predictive classification problem. GIS supplies the common spatial database within which environmental, hydrological, social, and infrastructural variables are aligned and analysed. AHP introduces transparent expert-based factor prioritization through pairwise comparisons and consistency testing. Machine learning estimates empirical associations between conditioning variables and observed flood occurrence and is capable of representing nonlinear relationships and interactions that may not be captured by additive weighted-overlay procedures. These three components represent different but complementary sources of analytical evidence. AHP is interpretable because the decision criteria, weights, and expert judgments can be examined directly, although its results may be affected by subjectivity, criteria dependence, classification thresholds, and assumptions of linear compensation. Machine-learning models can identify complex predictive patterns and generate probability-based susceptibility surfaces, although they may be affected by overfitting, sample imbalance, multicollinearity, poor flood-inventory quality, hyperparameter selection, and spatial autocorrelation. GIS allows both approaches to be applied to common spatial units, but the quality of the resulting maps remains dependent on raster resolution, projection consistency, positional accuracy, data completeness, and layer harmonization. Comparative flood research has shown that machine-learning algorithms frequently outperform conventional index-based approaches, although the best-performing method varies according to the terrain, sample size, predictor set, hydrological context, and validation procedure (Mosavi et al., 2018). Meta-heuristic optimization has further demonstrated that feature selection, model calibration, and parameter optimization can alter both predictive accuracy and the spatial distribution of susceptibility categories (Arabameri et al., 2022). Digital elevation model resolution has also been found to affect the performance of machine-learning models, confirming that algorithmic complexity cannot fully compensate for inadequate spatial representation (Avand et al., 2022). Integration can therefore involve comparing AHP-derived factor weights with machine-learning variable-importance measures, using AHP maps as baseline models, incorporating weighted factors as model inputs, or evaluating whether expert priorities correspond with empirical predictive relationships. High-resolution integrated modelling requires a reliable flood inventory, clearly defined flood and non-flood samples, standardized conditioning layers, separation of training and testing datasets, assessment of multicollinearity, cross-validation, hyperparameter optimization, and evaluation through accuracy, sensitivity, specificity, precision, recall, F1-score, receiver operating characteristic curves, and area-under-the-curve values. The model outputs may be continuous probability surfaces or susceptibility indices that are classified into ordered categories for comparison across communities, administrative units, or raster cells. The integration of objective spatial modelling with questionnaire-based assessment also permits geospatial data quality, AHP weighting effectiveness, machine-learning predictive capability, and GIS-AHP-ML integration capability to be examined as measurable constructs within the same quantitative case-study design.

Flood vulnerability refers to the susceptibility of exposed populations, buildings, infrastructure, economic activities, livelihoods, public services, and environmental systems to damage or disruption when a flood occurs. Vulnerability is multidimensional because locations exposed to the same flood depth or duration may experience very different levels of loss depending on income, age, education, housing quality, infrastructure condition, drainage capacity, emergency access, ecosystem health, and institutional preparedness. Social vulnerability includes demographic and socioeconomic characteristics that influence the ability of households and communities to anticipate, withstand, respond to, and recover from flooding. Economic vulnerability concerns income, employment, livelihood dependence, property ownership, business activity, and financial resources. Physical vulnerability refers to the resistance, location, construction quality, and exposure of buildings and infrastructure. Environmental vulnerability concerns ecosystem degradation, soil erosion, vegetation removal, wetland loss, and land-cover changes that reduce natural flood-buffering capacity. Infrastructural vulnerability concerns the exposure, condition, accessibility, and functional reliability of roads, bridges, drainage networks, electricity systems, water services, hospitals, schools, and emergency shelters. Indicator-based flood studies have transformed these dimensions into normalized indices that permit comparison among catchments, neighbourhoods, cities, and administrative units (Balica et al., 2009). Statistical validation of social-vulnerability indicators in German river-flood contexts demonstrated that demographic and socioeconomic variables could be reduced to interpretable components and tested against household-level flood experiences through regression analysis (Fekete, 2009). Integrated assessment in Rotterdam combined flood hazard, exposure, and social vulnerability and demonstrated that populations located within the same flood zone may differ considerably in their ability to prepare for, respond to, and recover from flood events (Koks et al., 2015). Flood-damage research has also emphasized that exposure and vulnerability must receive analytical attention comparable to hazard because flood depth and extent alone cannot explain observed economic and social losses (Merz et al., 2010). GIS-based multi-criteria vulnerability assessments have combined social, economic, physical, and environmental indicators to produce composite vulnerability surfaces. Sensitivity analysis has shown that changes in indicator selection and weighting can alter local vulnerability categories (Feizizadeh & Kienberger, 2017). Similar uncertainty analysis has demonstrated that housing quality, preparedness, and socioeconomic criteria may strongly influence the spatial stability of vulnerability maps (Brito et al., 2019). Integrated urban flood-risk analysis has further shown that environmental conditioning factors, exposure variables, and vulnerability indicators can be combined through GIS and AHP to identify spatial variations in risk (Ouma & Tateishi, 2014). Flood-risk classification must therefore remain analytically distinct from flood-susceptibility classification. Susceptibility identifies where flooding is more likely to occur, exposure identifies the people and assets located within those areas, vulnerability measures the likelihood of severe consequences, and risk classification combines these dimensions into categories such as very low, low, moderate, high, and very high.

The present study examines machine learning-enhanced GIS and AHP modelling for high-resolution flood-susceptibility prediction, multidimensional vulnerability assessment, and integrated flood-risk classification within a selected case-study area. It employs a quantitative, cross-sectional, explanatory, predictive, and case-study-based research design that combines objective spatial information with structured responses obtained from relevant professionals and stakeholders. The spatial component includes the development of a historical flood inventory and the preparation of conditioning-factor layers such as elevation, slope, rainfall, drainage density, distance from rivers, land use and land cover, soil, lithology, flow accumulation, topographic wetness, vegetation condition, road proximity, and infrastructure concentration. The AHP component determines expert-based factor weights through pairwise comparison, matrix normalization, priority-vector calculation, and consistency analysis. The machine-learning component trains and validates alternative predictive models using flood and non-flood observations. The vulnerability component measures social, economic, demographic, physical, environmental, and infrastructural conditions, while the risk-classification component integrates susceptibility, exposure, and vulnerability measures. The structured questionnaire uses a five-point Likert scale to measure geospatial and hydrological data quality and integration, AHP-based flood-conditioning factor weighting, machine-learning predictive capability, GIS-AHP-ML integration capability, socioeconomic and demographic vulnerability assessment, physical, environmental, and infrastructural vulnerability assessment, high-resolution flood-susceptibility prediction effectiveness, overall flood-vulnerability assessment effectiveness, and integrated flood-risk classification effectiveness. Descriptive statistics are used to determine the average level, distribution, and variability of each construct. Pearson correlation analysis is used to measure the direction and strength of the relationships among the study variables. Multiple regression analysis is used to estimate the individual and collective contribution of the independent variables while controlling for the influence of other predictors included in each model. Statistical validation of social-vulnerability constructs through regression analysis has previously demonstrated the relevance of quantitative hypothesis testing in flood research (Fekete, 2009). Comparative testing of multiple algorithms against the same flood inventory has also established the importance of evaluating predictive methods under consistent data and validation conditions (Khosravi et al., 2018). Sensitivity and uncertainty analyses have further shown the need to examine the robustness of spatial classifications and criteria-weighting procedures (Brito et al., 2019). The first regression model examines whether geospatial and hydrological data quality, AHP weighting effectiveness, machine-learning predictive capability, and GIS-AHP-ML integration capability influence high-resolution flood-susceptibility prediction effectiveness. The second model examines whether socioeconomic and demographic vulnerability assessment and physical, environmental, and infrastructural vulnerability assessment influence overall flood-vulnerability assessment effectiveness. The third model examines whether flood-susceptibility prediction effectiveness and vulnerability-assessment effectiveness influence integrated flood-risk classification effectiveness. The study therefore treats spatial data quality, expert weighting, predictive modelling, vulnerability measurement, and risk classification as interconnected but empirically distinguishable components of one integrated flood-analysis system.

Background of the Study

Flooding represents one of the most widespread and destructive natural hazards because it affects human settlements, transportation systems, agricultural land, public infrastructure, environmental resources, and local economic activities across diverse geographical regions. The severity of flood impacts is influenced not only by rainfall intensity or river overflow but also by elevation, slope, drainage characteristics, land-use patterns, soil conditions, vegetation loss, urban expansion, surface impermeability, and the concentration of vulnerable populations and assets. Conventional flood-assessment approaches have often depended on historical records, field observations, hydrological calculations, or generalized hazard maps that may not capture localized variations in terrain, drainage, and human settlement. Such limitations create difficulties for identifying small but highly exposed areas where floodwater may accumulate rapidly. Geographic Information Systems have become important in flood research because they allow multiple spatial datasets to be collected, processed, standardized, overlaid, and converted into interpretable flood-susceptibility maps. Remote sensing, digital elevation models, rainfall datasets, drainage networks, land-use maps, soil information, and historical flood locations can be integrated within a GIS environment to represent the spatial conditions associated with flood occurrence. The Analytic Hierarchy Process further supports this analysis by enabling experts to compare and assign relative weights to flood-conditioning factors through a structured pairwise comparison procedure. However, AHP-based weighted-overlay methods may not fully capture complex nonlinear relationships among environmental variables. Machine-learning techniques offer an additional predictive capability by learning patterns from historical flood and non-flood observations and estimating the likelihood of flooding across unsampled locations. The integration of machine learning, GIS, and AHP therefore creates a more comprehensive analytical structure in which expert knowledge, spatial evidence, and data-driven prediction can be examined together. High-resolution flood-susceptibility prediction is particularly important because localized topographic depressions, drainage blockages, road embankments, channel proximity, and land-cover changes may be hidden within coarse spatial datasets. Flood-risk assessment also requires more than the prediction of flood-prone locations because communities and infrastructure exposed to similar hazards may experience different levels of damage. Social, economic, demographic, physical, environmental, and infrastructural vulnerability must consequently be assessed alongside flood susceptibility. This research has been developed to integrate these interconnected dimensions within a quantitative, cross-sectional, case-study-based framework that applies GIS, AHP, machine learning, descriptive statistics, Pearson correlation analysis, regression modelling, and a five-point Likert scale to evaluate the effectiveness of high-resolution flood prediction, vulnerability assessment, and risk classification.

Problem Statement

Flood-risk management frequently depends on maps and assessments that present generalized hazard zones without adequately representing the localized environmental, hydrological, social, and infrastructural conditions that determine where flooding is likely to occur and where its consequences may be most severe. Many conventional flood-susceptibility studies rely on weighted spatial overlays in which flood-conditioning factors are assigned fixed values based on expert judgment or previously established assumptions. Although these methods provide understandable and visually useful outputs, their predictive ability may be weakened when complex interactions among rainfall, elevation, slope, drainage density, river proximity, soil, land use, vegetation, and urban development are treated as simple linear relationships. Expert-based weighting can also be affected by subjective preferences, inconsistency among evaluators, limited local knowledge, and uncertainty regarding the relative importance of different conditioning variables. At the same time, machine-learning models may produce high predictive accuracy while offering limited transparency concerning how individual factors influence the final classification. Their performance can also be reduced by incomplete flood inventories, imbalanced training samples, coarse spatial resolution, correlated predictors, overfitting, and inadequate model validation. Another major problem is that flood susceptibility is often treated as equivalent to flood risk, even though susceptibility indicates the likelihood of flooding while risk also depends on exposure and vulnerability. An area classified as highly susceptible may contain few people or assets, while a moderately susceptible area may create serious consequences because of dense settlement, weak drainage, fragile infrastructure, poverty, limited transportation access, and insufficient emergency services. Separate treatment of susceptibility and vulnerability can therefore produce incomplete classifications and may fail to identify locations where physical flood probability and human vulnerability overlap. In addition, many existing studies focus primarily on spatial modelling and do not examine how professionals and stakeholders evaluate geospatial data quality, AHP weighting effectiveness, machine-learning capability, model integration, vulnerability measurement, and risk-classification performance. This limits the ability to test the operational and organizational dimensions of integrated flood modelling through statistical analysis. A research gap consequently exists regarding the combined use of high-resolution GIS data, consistent AHP weighting, validated machine-learning models, multidimensional vulnerability indicators, and quantitative stakeholder assessments within a single case-study framework. Without such integration, flood-management authorities may receive maps that are spatially detailed but socially incomplete, statistically accurate but difficult to interpret, or methodologically transparent but insufficiently predictive. The central problem addressed by this research is therefore the absence of a unified and empirically testable framework that combines geospatial data, expert knowledge, machine-learning prediction, vulnerability assessment, and risk classification to identify and differentiate flood-prone and flood-vulnerable locations at a high spatial resolution.

Objectives of The Study

The principal objective of this study is to develop and evaluate an integrated machine learning-enhanced GIS and AHP framework for high-resolution flood-susceptibility prediction, multidimensional vulnerability assessment, and flood-risk classification within the selected case-study area. To achieve this objective, the research first seeks to examine the quality, completeness, spatial resolution, consistency, and integration of the geospatial and hydrological datasets used in the modelling process. This includes determining whether elevation, slope, rainfall, river proximity, drainage density, land use and land cover, soil, vegetation, flow accumulation, and other relevant factors are sufficiently accurate and compatible for high-resolution spatial analysis. The study also aims to assess the effectiveness of AHP-based weighting by examining the suitability of the selected flood-conditioning factors, the consistency of expert pairwise comparisons, and the relative importance assigned to each criterion. Another objective is to evaluate the predictive capability of selected machine-learning algorithms and compare their performance using suitable training, testing, validation, and classification measures. The research further seeks to determine whether the integration of GIS, AHP, and machine learning produces a stronger and more reliable flood-susceptibility assessment than the separate application of individual modelling techniques. In relation to vulnerability, the study aims to assess how social, economic, demographic, physical, environmental, and infrastructural conditions influence the ability of communities and systems to withstand flood events. It also seeks to measure the effectiveness of combining these vulnerability dimensions into a comprehensive assessment that distinguishes areas with different levels of sensitivity and coping capacity. A further objective is to examine the statistical relationships among geospatial data quality, AHP weighting, machine-learning capability, model integration, flood-susceptibility prediction, vulnerability assessment, and risk-classification effectiveness. Descriptive statistics will be used to summarize respondents' evaluations of the principal constructs, Pearson correlation analysis will determine the direction and strength of the relationships among variables, and multiple regression modelling will estimate the independent and collective influence of the predictors. The study also aims to classify the selected area into very low, low, moderate, high, and very high flood-susceptibility, vulnerability, and risk categories. Through these objectives, the research will systematically connect spatial prediction with human and infrastructural conditions while maintaining clear distinctions among flood susceptibility, exposure, vulnerability, and risk. The resulting analytical structure will allow the stated research questions and hypotheses to be examined through both geospatial modelling and quantitative statistical evidence.

Research Hypotheses

The research hypotheses have been formulated to test the proposed relationships among the technological, spatial, analytical, and vulnerability-related constructs included in the study. The first hypothesis, H1, states that geospatial and hydrological data quality and integration have a statistically significant positive effect on high-resolution flood-susceptibility prediction effectiveness. This hypothesis assumes that accurate, complete, current, high-resolution, and properly aligned spatial datasets improve the reliability of flood prediction. The second hypothesis, H2, states that AHP-based flood-conditioning factor weighting has a statistically significant positive effect on high-resolution flood-susceptibility prediction effectiveness. It examines whether systematic factor selection, pairwise comparison, consistency checking, and appropriate weight assignment improve the resulting susceptibility model. The third hypothesis, H3, proposes that machine-learning predictive capability has a statistically significant positive effect on high-resolution flood-susceptibility prediction effectiveness. This relationship focuses on the contribution of algorithm selection, data preparation, model training, cross-validation, hyperparameter optimization, and predictive accuracy. The fourth hypothesis, H4, states that GIS-AHP-machine-learning integration capability has a statistically significant positive effect on high-resolution flood-susceptibility prediction effectiveness. It evaluates whether the coordinated use of spatial processing, expert weighting, and data-driven modelling strengthens the final predictive output. The fifth hypothesis, H5, proposes that social, economic, and demographic vulnerability assessment has a statistically significant positive effect on overall flood-vulnerability assessment effectiveness. This hypothesis considers indicators such as population density, age, education, income, employment, dependency, and access to resources. The sixth hypothesis, H6, states that physical, environmental, and infrastructural vulnerability assessment has a statistically significant positive effect on overall flood-vulnerability assessment effectiveness. It examines the contribution of building conditions, drainage capacity, roads, utilities, vegetation, land degradation, and access to critical facilities. The seventh hypothesis, H7, proposes that high-resolution flood-susceptibility prediction effectiveness has a statistically significant positive effect on integrated flood-risk classification effectiveness. The eighth hypothesis, H8, states that flood-vulnerability assessment effectiveness has a statistically significant positive effect on integrated flood-risk classification effectiveness. Collectively, these hypotheses establish three linked analytical models: the first predicts flood-susceptibility effectiveness from data quality, AHP weighting, machine-learning capability, and model integration; the second predicts vulnerability-assessment effectiveness from social and physical vulnerability dimensions; and the third predicts flood-risk classification effectiveness from susceptibility-prediction and vulnerability-assessment effectiveness. Each hypothesis will be tested using Pearson correlation analysis and multiple regression modelling at an appropriate statistical significance level.

Significance of the Research

i. **Significance for disaster-management authorities:** The study will provide disaster-management agencies with a structured approach for identifying locations where flood occurrence is more likely and where exposed populations and infrastructure may experience serious consequences. The classification of areas into very low, low, moderate, high, and very high risk categories can support the prioritization

of preparedness, response, evacuation, and recovery activities.
ii. **Significance for local government and urban planning:** Local government institutions and planning authorities can use high-resolution susceptibility and risk information to evaluate land-use decisions, settlement expansion, drainage improvement, road construction, public-facility location, and floodplain management. The distinction between susceptibility and vulnerability can help planners avoid treating all flood-prone areas as equally risky.
iii. **Significance for GIS and hydrological professionals:** The research will demonstrate how geospatial data quality, spatial resolution, factor standardization, raster alignment, expert weighting, and machine-learning validation influence flood-modelling effectiveness. This can assist technical professionals in improving data-processing procedures and selecting suitable modelling approaches.
iv. **Significance for machine-learning applications:** The study will provide a basis for comparing selected machine-learning algorithms within a common flood inventory and conditioning-factor dataset. It will also show how machine-learning outputs can be interpreted alongside AHP-derived factor weights and GIS-based spatial patterns rather than being treated as isolated predictive results.
v. **Significance for vulnerable communities:** By incorporating social, economic, demographic, physical, environmental, and infrastructural indicators, the research will represent the different capacities of communities to prepare for, respond to, and recover from flooding. This allows risk classification to consider both physical flood likelihood and the conditions that increase human suffering and service disruption.
vi. **Significance for infrastructure management:** Roads, bridges, drainage networks, electricity systems, water facilities, hospitals, schools, and emergency shelters can be assessed according to their location within susceptibility and vulnerability zones. This information can support the identification of critical facilities requiring protection, maintenance, reinforcement, or improved accessibility.
vii. **Significance for academic research:** The study will contribute an integrated quantitative framework that combines GIS, AHP, machine learning, vulnerability assessment, descriptive statistics, Pearson correlation, and multiple regression analysis. It will also provide measurable constructs and testable hypotheses that connect technical flood modelling with stakeholder evaluations of modelling effectiveness.
viii. **Significance for policy formulation:** The results can assist policymakers in developing evidence-based floodplain regulations, risk-sensitive development controls, data-sharing procedures, infrastructure investment priorities, and community preparedness measures. The integrated framework can also support more transparent explanations of why particular locations receive higher flood-risk classifications than others.

LITERATURE REVIEW

The literature on flood-susceptibility prediction, vulnerability assessment, and risk classification has developed through several interconnected areas of investigation, including hydrological analysis, Geographic Information Systems, remote sensing, multi-criteria decision analysis, machine learning, social-vulnerability measurement, and disaster-risk theory. Flood research initially concentrated heavily on the physical characteristics of inundation, such as river discharge, rainfall intensity, flood depth, flow velocity, and return periods. Broader spatial assessments have increasingly recognized that flood occurrence and flood consequences are influenced by a larger set of environmental and human factors. Elevation, slope, drainage density, river proximity, land use and land cover, soil characteristics, geology, vegetation, flow accumulation, and urban surface conditions are commonly examined as flood-conditioning variables because they influence runoff generation, water concentration, infiltration, and drainage efficiency. GIS and remote-sensing techniques have allowed these factors to be represented as spatial layers and combined to produce flood-susceptibility maps. Multi-criteria methods such as the Analytic Hierarchy Process have supported this work by providing a structured procedure for selecting, comparing, and weighting multiple conditioning factors. However, the dependence of AHP on expert judgment has led researchers to examine consistency, sensitivity, and uncertainty within pairwise comparisons and weighted-overlay results. Machine-learning methods have expanded flood research by enabling models to learn complex and nonlinear relationships from historical flood and non-flood observations. Algorithms such as random forest, support vector machine, logistic regression, decision tree, artificial neural network, gradient boosting, and neuro-fuzzy systems have been used to generate probability-based susceptibility surfaces and compare predictive performance. The literature also indicates that susceptibility does not independently represent flood risk because risk depends on the interaction of hazard or susceptibility with exposure and vulnerability. Social, economic, demographic, physical, environmental, and infrastructural indicators are therefore used to explain why communities exposed to similar flood conditions may experience different levels of damage, disruption, and recovery difficulty. The Pressure and Release Model of Disaster Risk provides a theoretical basis for examining how hazardous physical conditions interact with socially produced vulnerability and unsafe conditions. A corresponding conceptual framework can connect geospatial data quality, AHP weighting, machine-learning capability, model integration, flood-susceptibility prediction, vulnerability assessment, and risk classification. The literature review will therefore examine six principal areas: the concepts of flood susceptibility, vulnerability, exposure, and risk; GIS, remote sensing, and high-resolution mapping; AHP-based flood-conditioning factor weighting; machine-learning models for flood prediction; the Pressure and Release Model as the theoretical framework; and the integrated conceptual framework and hypothesized relationships guiding the study.

Flood Susceptibility, Vulnerability, Exposure, and Risk Classification

Flood susceptibility, vulnerability, exposure, and risk represent related but analytically distinct concepts within flood assessment. Flood susceptibility describes the relative tendency of a location to experience inundation because of its topographic, hydrological, and land-use characteristics. It indicates where flooding is more likely to occur without calculating probability, depth, velocity, duration, or economic consequence of an event. Flood hazard is broader because it may incorporate the probability, frequency, magnitude, depth, velocity, and spatial extent of inundation. Exposure refers to the people, households, buildings, roads, utilities, agricultural land, public facilities, and resources situated in places that may be affected. Vulnerability expresses the degree to which those exposed elements are susceptible to injury, loss, disruption, or reduced functioning. Risk emerges when the physical possibility of flooding intersects with exposed values and their vulnerability. This relationship has been represented as a combination of hazard, exposed values, and vulnerability, emphasizing that losses cannot be explained by the flood process alone (Kron, 2005; Kanti, 2020). A highly susceptible floodplain may have limited risk when it contains few people or assets, while a moderately susceptible urban zone may have substantial risk when it contains dense settlement, expensive infrastructure, weak drainage, and disadvantaged households. The distinction also prevents susceptibility maps from being interpreted as complete risk maps. Global disaster assessment has operationalized this separation by modelling hazards spatially, overlaying them with population distribution to estimate exposure, and associating observed human losses with socioeconomic and environmental characteristics used to represent vulnerability (Debasish, 2021; Peduzzi et al., 2009). Such differentiation is important for this research because the GIS and machine-learning components estimate high-resolution flood susceptibility, whereas the vulnerability and exposure components describe severity and distribution of consequences. The final classification must preserve the conceptual boundaries among physical flood likelihood, the location of valued elements, their susceptibility to harm, and the level of flood risk.

Vulnerability is multidimensional and context dependent because the same flood intensity can generate different consequences across populations and places. Physical vulnerability concerns the location, materials, elevation, condition, and resistance of buildings, roads, bridges, drainage systems and utilities. Social vulnerability includes age, disability, health, education, household structure and access to information. Economic vulnerability reflects income, employment, livelihood dependence, savings, property ownership, insurance, and the capacity to finance evacuation, repair, relocation, and recovery. Environmental vulnerability concerns wetland loss, vegetation degradation, soil erosion, channel modification, pollution, and declining ecosystem functions that increase runoff or reduce natural buffering capacity. Institutional and infrastructural conditions influence warning dissemination, emergency access, shelter availability, service continuity, and the speed with which communities restore normal activities. Integrative disaster-risk frameworks have represented vulnerability through exposure, susceptibility or fragility, resilience, coping capacity, and adaptive capacity rather than treating it as a fixed property (Birkmann et al., 2013; Abdur & Iftekhar, 2021). A composite vulnerability score should represent several dimensions while retaining a rationale for indicator selection, normalization, weighting, and aggregation. A review of 67 flood-disaster case studies identified demographic characteristics, socioeconomic status, and health as drivers of social vulnerability, while showing that risk perception and coping capacity were often insufficiently represented in standardized indices (Sheak & Risha, 2022; Rufat et al., 2015). Exposure is more complex than the presence of population within a mapped flood zone. The number of people, building type, infrastructure function, economic value, and dependence on essential services influence the consequences associated with a location. In GIS analysis, exposure can be represented through gridded population, settlement footprints, road networks, public facilities, agricultural areas, and referenced assets. Vulnerability indicators can be attached to administrative units, communities, households, or raster cells, provided that differences in scale and resolution are addressed. This approach differentiates locations with similar susceptibility according to social fragility, physical condition and capacity to withstand flooding.

Figure 2: Design Science Research Framework for Integrated Flood Susceptibility and Risk Classification

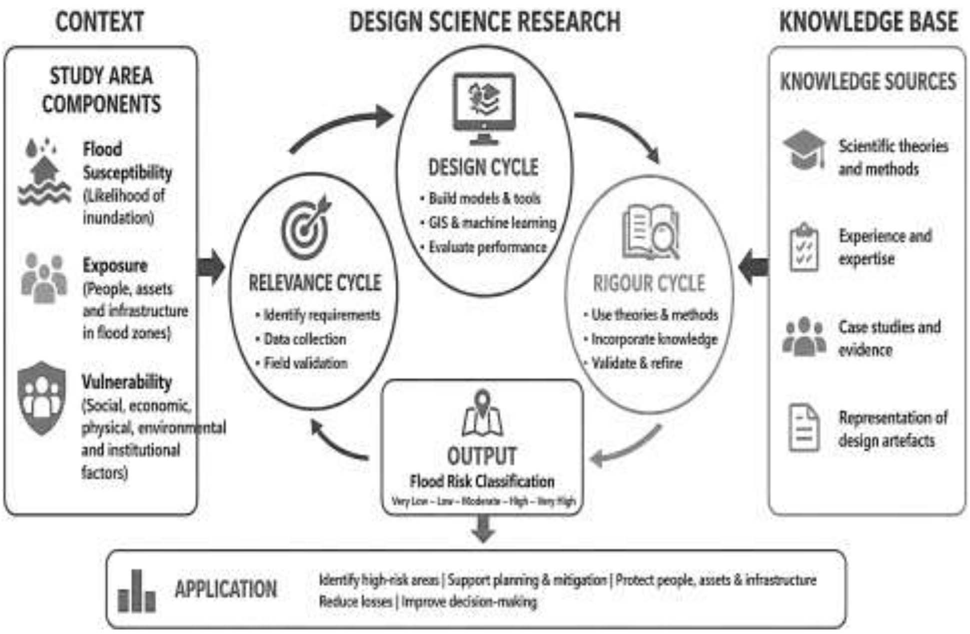

Flood-risk classification translates measurements into ordered categories that communicate levels of concern across a study area. A classification may contain very low, low, moderate, high, and very high classes, although the meaning of each class depends on the variables, weights, thresholds, and spatial units used. Susceptibility classification converts modelled probabilities or index scores into zones indicating the relative likelihood of flood occurrence. Vulnerability classification arranges social, economic, physical, environmental, and infrastructural conditions according to their potential for harm. Exposure classification represents the concentration or value of people and assets within affected areas. Risk classification integrates these components to identify locations where flood likelihood and consequences overlap. The classes may be generated through natural breaks, quantiles, equal intervals, standard deviations, expert-defined thresholds, fuzzy membership functions, or multi-criteria combinations. Each method can produce a spatial distribution, so the classification rule must be reported and evaluated against historical flood information, field evidence, or independent observations. GIS-based flood-risk assessment has demonstrated how physical vulnerability, social vulnerability, and coping capacity can be integrated through the Analytic Hierarchy Process and weighted linear combination to produce composite vulnerability and risk zones (Dandapat & Panda, 2017; Chowdhury & Tonay, 2022). Their assessment reported that 24.25 percent of the population in the examined district lived in high to very high flood-risk zones, showing how categorical maps summarize the intersection of hazard and vulnerability. For this study, high-resolution susceptibility prediction will be generated from geospatial conditioning factors, AHP-derived weights, and machine-learning outputs, while vulnerability will be assessed through social, economic, demographic, physical, environmental, and infrastructural indicators. The integrated risk classes will represent combinations of physical susceptibility, exposed elements, and differentiated capacities for damage and disruption. Statistical analysis of stakeholder responses will complement the spatial classification by testing whether data quality, weighting effectiveness, machine-learning capability, vulnerability assessment, and susceptibility prediction are associated with risk-classification effectiveness.

GIS and High-Resolution Flood-Susceptibility Mapping

Geographic Information Systems provide the principal spatial environment for organizing, transforming, analysing, and displaying the diverse datasets required for flood-susceptibility mapping. A GIS-based workflow normally begins with the collection of topographic, hydrological, climatic, geological, environmental, and anthropogenic information from digital elevation models, satellite imagery, rainfall records, river networks, soil maps, land-use databases, and historical flood inventories. These sources are converted into compatible raster or vector layers, projected into a common coordinate system, resampled to a consistent cell size, and clipped to the selected case-study boundary. From these data, researchers derive flood-conditioning factors such as elevation, slope, curvature, flow accumulation, drainage density, distance from rivers, topographic wetness, rainfall, soil permeability, vegetation condition, road proximity, and impervious-surface coverage. The spatial relationship between these factors and recorded flood locations can then be examined through overlay operations, map algebra, zonal statistics, and predictive modelling. Remote sensing strengthens this process by supplying repeated and geographically extensive observations of land cover, surface water, vegetation, urban expansion, and flood extent. Radar data are particularly useful because cloud cover and rainfall frequently limit optical imagery during flood events. A major review of flood-modelling research showed that remotely sensed flood-extent and water-stage information can support model calibration, validation, parameter estimation, and evaluation rather than serving only as descriptive post-event mapping evidence (Zahidul & Begum, 2022; Schumann et al., 2009). High-resolution flood mapping also depends on the ability to represent channels, floodplains, and terrain controls at spatial scales fine enough to preserve local hydrological variation. A global hydraulic model developed at approximately 90-metre resolution demonstrated that careful terrain processing, subgrid channel representation, and validation against detailed benchmark datasets could identify a substantial proportion of mapped flood-hazard areas across data-rich and data-scarce regions (Nishat & Kaniz, 2022; Sampson et al., 2015). GIS therefore connects raw observations, derived conditioning factors, predictive outputs, and mapped susceptibility classes within one spatially consistent analytical system.

Remote-sensing technologies contribute to flood-susceptibility research in two connected ways: they provide conditioning variables describing the landscape before flooding and observational evidence showing where inundation has occurred. Multispectral imagery can be classified to identify built-up land, cropland, forest, wetlands, open water, bare soil, and other land-cover categories that influence infiltration and runoff. Vegetation indices can represent surface cover and moisture conditions, while time-separated images can reveal urban growth and wetland conversion that alter drainage behaviour. Synthetic Aperture Radar is highly valuable for flood-inventory preparation because smooth open water usually produces low backscatter and can often be distinguished from surrounding land under cloudy and low-light conditions. Automated Sentinel-1 processing has shown that satellite radar scenes can be converted into flood maps rapidly while maintaining high thematic accuracy across test locations, supporting consistent delineation of observed inundation for model training and validation (Twele et al., 2016). The spatial resolution of these inputs directly affects the detail and reliability of the susceptibility surface. Coarse cells may merge riverbanks, drainage channels, roads, embankments, depressions, and adjacent land-cover types into generalized values, whereas finer cells can retain small-scale controls on water movement. A continental flood model produced at approximately 30-metre resolution achieved strong agreement with detailed governmental hazard products, particularly where comparison data were generated from high-quality local hydraulic studies, demonstrating that broad spatial coverage can be combined with decision-relevant detail when topography, levees, river flows, and rainfall are represented appropriately (Wing et al., 2017). High resolution should not be interpreted only as a small pixel size. It also requires adequate vertical accuracy in elevation data, precise geolocation, realistic drainage representation, current land-cover information, and compatible temporal coverage among datasets. Errors in these elements can propagate through derived factors and create misleading boundaries between susceptibility classes. Remote-sensing products must therefore be preprocessed through geometric correction, speckle reduction, cloud masking, mosaicking, classification, and accuracy assessment before incorporation into GIS-based flood models.

Figure 3: Methodological Framework for GIS, Remote Sensing, and High-Resolution Flood Susceptibility Mapping

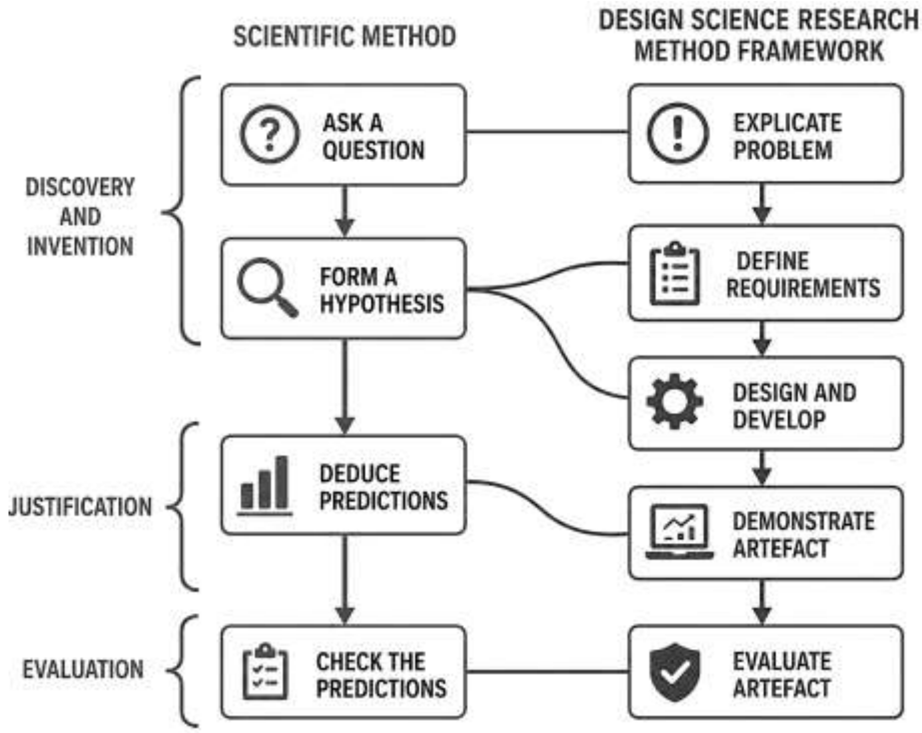

The development of a high-resolution flood-susceptibility map requires a systematic transition from spatial-data preparation to model construction, validation, interpretation, and classification. The first requirement is a reliable flood inventory containing geographically accurate flood and non-flood observations. Inventory points may be derived from historical records, field surveys, satellite-detected inundation, governmental reports, and community evidence, but duplicate, uncertain, or spatially biased observations must be identified before modelling. Conditioning-factor values are extracted for each observation, and the resulting database is examined for missing information, multicollinearity, class imbalance, and scale differences. GIS supports these procedures by linking every observation to the same set of raster predictors and enabling the trained model to be applied continuously across the study area. Remote sensing can increase inventory coverage where gauge networks and field records are incomplete. One study used Sentinel-1 imagery to identify flood locations and integrated them with eleven conditioning factors before comparing decision-table models optimized through genetic algorithms, particle swarm optimization, and harmony search, illustrating how remotely sensed inventories can be connected directly to GIS and machine-learning workflows (Askar et al., 2022). Validation remains essential because visually detailed maps may still contain systematic errors. Training and testing samples should be separated, spatial cross-validation should be considered when observations are clustered, and predictive performance should be reported through measures such as accuracy, sensitivity, specificity, precision, recall, F1-score, receiver operating characteristic curves, and area under the curve. The continuous prediction surface must then be divided into susceptibility classes using a clearly reported method, such as natural breaks, quantiles, equal intervals, or probability thresholds. Class areas, settlement exposure, infrastructure concentration, and agreement with independent flood observations can be calculated through GIS overlays. For the present research, GIS and remote sensing form the data and mapping foundation upon which AHP weighting and machine-learning prediction operate. Their effectiveness will be assessed through spatial-data quality, inventory reliability, model validation, resolution consistency, and the capacity of the final susceptibility classes to distinguish localized flood-prone areas.

AHP-Based Weighting of Flood-Conditioning Factors

The Analytic Hierarchy Process is a structured multi-criteria decision-making method used to convert complex judgments about flood-conditioning factors into a transparent system of relative priorities. In a flood-susceptibility study, the overall objective is normally placed at the highest level of the hierarchy, environmental and hydrological criteria are positioned at the intermediate level, and factor classes or spatial alternatives are placed at the lowest level. Experts compare every criterion with the remaining criteria by using a reciprocal pairwise scale that expresses equal, moderate, strong, very strong, or extreme importance. The comparison matrix is normalized, the principal eigenvector is calculated, and the resulting priority values become the weights assigned to the corresponding GIS layers. These weights enable factors measured in different units, such as millimetres of rainfall, degrees of slope, metres of elevation, kilometres of drainage proximity, and categorical land use, to be incorporated within one composite susceptibility index. The reliability of the judgments is evaluated through the Consistency Index and Consistency Ratio, which identify whether the comparisons follow a logically coherent pattern. A low Consistency Ratio does not prove that the selected weights are objectively correct, but it confirms that the expert judgments are internally consistent enough for spatial modelling. Research conducted in the Malda district used AHP to combine morphological and hydrometeorological hazard elements with demographic, socioeconomic, and infrastructural vulnerability indicators, illustrating how the method can separate hazard and vulnerability before integrating them into a flood-risk surface (Ghosh & Kar, 2018). A related district-level assessment in Coochbehar calculated flood hazard, vulnerability, and risk indices through AHP and GIS, showing that the relative influence of hazard and vulnerability varied among settlements and administrative subdivisions (Chakraborty & Mukhopadhyay, 2019). These applications demonstrate that AHP is not limited to ranking physical flood factors because its hierarchical structure can incorporate susceptibility, exposure, vulnerability, and coping-related criteria when their conceptual roles are clearly defined.

The quality of AHP-based flood mapping depends heavily on the selection, standardization, and spatial representation of the conditioning factors entered into the hierarchy. Elevation usually receives a high priority because low-lying terrain promotes water accumulation, while slope influences runoff velocity, infiltration opportunity, and the residence time of surface water. Distance from rivers represents exposure to channel overflow, drainage density reflects the concentration and conveyance of runoff, and flow accumulation indicates locations toward which water is topographically directed. Rainfall supplies the principal hydrometeorological input, whereas soil texture, geology, and land use influence permeability, storage, surface roughness, and runoff generation. Topographic wetness, stream power, curvature, ruggedness, vegetation, road density, and impervious surfaces can be included when data quality and the characteristics of the case-study area justify their use. Each continuous layer must be reclassified into ordered susceptibility classes before weighted overlay, and the direction of influence must be defined carefully. Lower elevations or shorter river distances may receive higher susceptibility ratings, while greater vegetation cover or more permeable soils may receive lower ratings. A large-scale investigation of the Western Ghat coastal belt integrated eleven environmental conditioning factors and four socioeconomic parameters through AHP, reported a Consistency Ratio of 0.0854 for the susceptibility matrix, and achieved an area-under-the-curve value of 0.84 during map validation (Das, 2020). The study demonstrated that AHP could manage a relatively large group of multi-source criteria when the hierarchy, pairwise comparisons, and class ratings were systematically documented. A data-scarce river-basin assessment also combined slope, river distance, land use and land cover, soil, drainage density, rainfall, population density, crop production, and road-river intersections to construct hazard, vulnerability, and risk indices (Ramkar & Yadav, 2021). This approach is particularly relevant where detailed hydraulic measurements are unavailable because AHP allows expert knowledge and accessible spatial datasets to be organized into an operational flood-assessment model without treating missing hydrodynamic information as equivalent to the absence of flood risk.

Figure 4: AHP Decision-Making Process for Flood-Conditioning Factor Prioritization

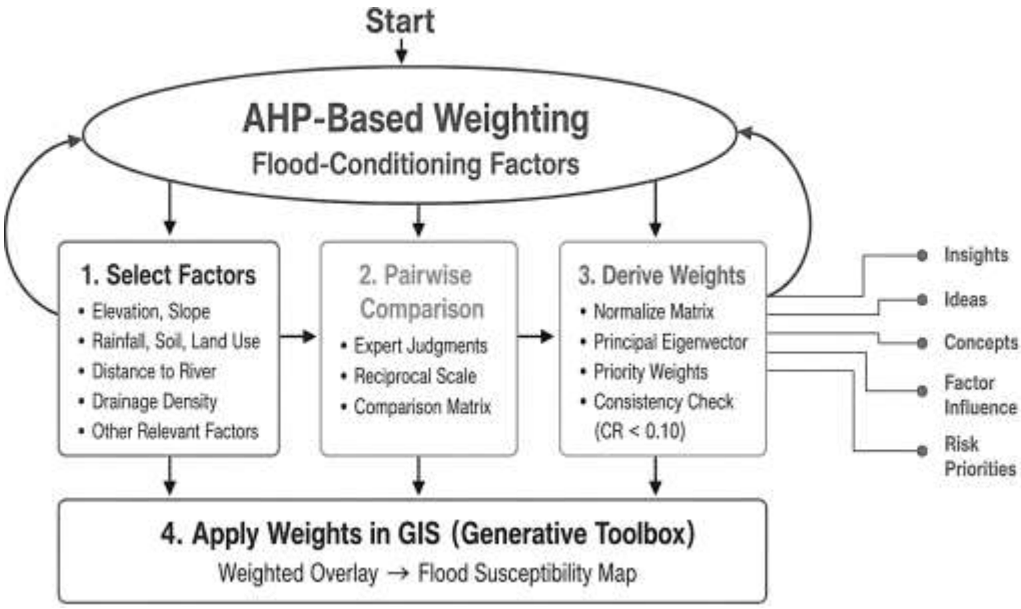

AHP-based weighting remains sensitive to the identity of the experts, the wording of the comparison questions, the number of criteria, the classification of factor values, and the assumption that individual criteria can compensate for one another through weighted addition. Two specialists may assign different priorities because they understand the local flood process differently, and increasing the number of factors creates a larger comparison matrix that may produce judgment fatigue or inconsistency. Correlated criteria can also receive separate weights even when they describe overlapping hydrological processes, which may unintentionally magnify their contribution to the final index. Factor selection should therefore be supported by the flood mechanisms operating within the study area, previous empirical evidence, data availability, and preliminary statistical examination. Expert panels should include professionals with knowledge of hydrology, GIS, remote sensing, environmental management, urban planning, and local flood history. Individual matrices may be aggregated through geometric means, after which the Consistency Ratio should be calculated and inconsistent judgments revised. Sensitivity analysis can test whether modest changes in factor weights produce major shifts in susceptibility classes, while comparison with historical flood locations can determine whether high-weight combinations correspond to observed inundation. AHP can also be combined with data-driven methods to reduce dependence on expert judgment. A study in Kastamonu compared standalone AHP, frequency ratio, and an AHP-frequency-ratio ensemble using eleven conditioning variables and remotely identified flood points. The reported area-under-the-curve values were 0.965, 0.989, and 0.992, respectively, indicating that the ensemble provided the strongest discrimination for that case-study dataset (Yilmaz, 2022). Such comparisons show that AHP weights can function as an interpretable expert baseline while statistical evidence adjusts or verifies the strength of factor relationships. In the present research, AHP will therefore be applied through explicit factor selection, pairwise comparison, matrix normalization, priority-weight calculation, consistency testing, weighted GIS overlay, susceptibility classification, sensitivity checking, and comparison with machine-learning predictions. This procedure preserves the transparency of expert reasoning while allowing its spatial output to be evaluated against observed flood records and predictive performance measures.

Machine-Learning Models for Flood-Susceptibility Prediction

Machine-learning models support flood-susceptibility research because they can identify complex statistical relationships between recorded flood occurrence and the environmental conditions represented within a geographic information system. A typical modelling database contains flood and non-flood observations as the dependent classes and a set of conditioning variables, including elevation, slope, rainfall, drainage density, distance from rivers, land use, soil, lithology, curvature, flow accumulation, vegetation, and topographic wetness, as predictors. Supervised algorithms learn from these labelled examples and assign each raster cell a probability or class indicating its relative tendency to experience flooding. Random forest constructs numerous decision trees from bootstrap samples and randomized predictor subsets, then aggregates their outputs to reduce variance and model nonlinear interactions. Boosted trees build trees sequentially, with later learners emphasizing errors made by earlier learners, thereby improving discrimination in difficult portions of the predictor space. An urban study in Seoul used twelve topographic, geological, soil, and land-use variables, trained models with flooded areas recorded in 2010, and validated them with independent flooding from 2011; random-forest classification attained 79.18 percent validation accuracy, slightly exceeding the tested boosted-tree alternatives (Lee et al., 2017). Ensemble modelling can also combine algorithms that represent relationships differently rather than relying on one learner. Multivariate discriminant analysis, classification and regression trees, and support vector machines were applied to the same watershed database, and only models exceeding a defined accuracy threshold were retained in the ensemble; slope, drainage density, and river distance emerged as influential predictors (Choubin et al., 2019). These studies indicate that algorithm comparison should use an identical inventory, predictor set, training partition, and validation sample. Otherwise, differences attributed to algorithms may actually reflect data quality, spatial resolution, sampling design, or inconsistent evaluation procedures. Machine-learning susceptibility mapping therefore requires computational capability and carefully controlled geospatial design that preserves comparability among candidate models.

Figure 5: Machine-Learning Framework for Flood-Susceptibility Prediction and Model Evaluation

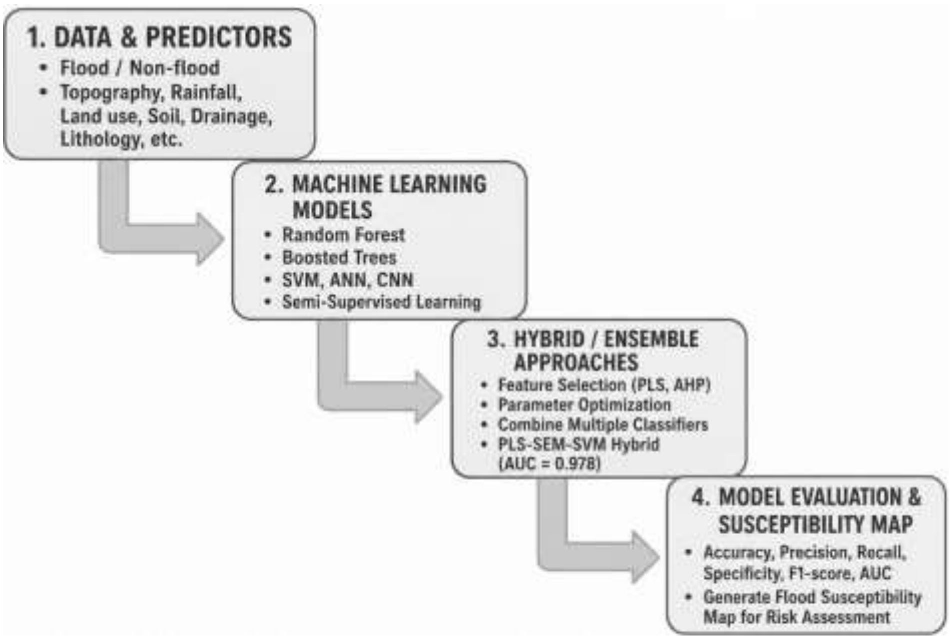

Support vector machines, artificial neural networks, and deep-learning models represent flood boundaries and interactions that conventional linear methods may miss. A support vector machine identifies a decision boundary that maximizes separation between flood and non-flood observations, while kernel functions allow this boundary to be transformed for nonlinear classification. Its effectiveness may decline when labelled flood inventories are small, spatially clustered, or incomplete.

Semi-supervised learning addresses this limitation by using labelled and unlabelled observations. A weakly labelled support vector machine developed for metropolitan Beijing incorporated flood records from 2004 to 2014 and nine meteorological, geographical, and anthropogenic factors; it outperformed logistic regression, artificial neural networks, and a conventional support vector machine across accuracy, precision, recall, F-score, and receiver operating characteristic evaluation (Zhao et al., 2019). Artificial neural networks learn weighted connections among input factors through hidden units, while deep architectures introduce multiple representation layers that can detect increasingly complex combinations of terrain and hydrological characteristics. Convolutional neural networks are relevant because they can retain information concerning the spatial neighbourhood surrounding a cell rather than treating each observation as independent. A convolutional framework for flood susceptibility demonstrated that the organization of surrounding spatial information can support accurate classification and can reveal nonlinear interactions among conditioning factors (Wang et al., 2020). These models nevertheless require careful architecture selection, regularization, parameter tuning, and computational management. Excessive network complexity may memorize the training sample, while limited complexity may fail to represent the underlying relationships. Class imbalance is also important because non-flood cells often greatly outnumber observed flood cells, allowing a model to produce high overall accuracy while poorly identifying the hazardous class. Balanced sampling, class weights, resampling procedures, and threshold analysis should therefore accompany neural and kernel-based modelling. Their performance should be assessed on withheld observations through several complementary measures rather than training accuracy alone.

Hybrid and ensemble machine-learning approaches seek to strengthen flood-susceptibility prediction by linking feature evaluation, statistical modelling, optimization, and multiple classifiers within an analytical framework. Hybridization may occur when a statistical method selects significant predictors before machine-learning training, when a metaheuristic algorithm optimizes parameters, when expert-derived AHP scores are supplied as inputs, or when the predictions of several base learners are combined. These designs matter because algorithms have different strengths and errors. Decision trees are interpretable but may be unstable, support vector machines can classify complex boundaries but require parameter selection, nearest-neighbour methods are flexible but sensitive to distance measures and scaling, and neural networks capture nonlinear patterns but may be difficult to interpret. A 2022 study integrated partial least squares structural equation modelling with multilayer perceptron neural networks, k-nearest neighbour, support vector machines, and radial-basis-function networks; the PLS-SEM-SVM hybrid achieved an area under the receiver operating characteristic curve of 0.978 and exceeded the alternative combinations (Mishra et al., 2022). This result shows the value of identifying influential flood factors before final classification. However, higher accuracy does not establish generalizability. Random splitting may place nearby cells in both training and testing datasets, enabling spatial autocorrelation to inflate performance. Spatial cross-validation, independent-event validation, and testing in geographically separated zones provide evidence. Predictor multicollinearity, missing values, differing measurement scales, inventory uncertainty, and data leakage must also be examined before training. Model interpretation can be supported through variable-importance scores, partial-dependence analysis, permutation tests, sensitivity analysis, and comparison with AHP-derived priorities. For the present research, machine-learning models should be trained on harmonized high-resolution GIS layers, evaluated with the same flood inventory, and compared through accuracy, precision, recall, specificity, F1-score, kappa, and area under the curve. The strongest model should then generate the susceptibility surface used alongside vulnerability and exposure information for integrated risk classification.

Theoretical Framework: Pressure and Release Model of Disaster Risk

The Pressure and Release Model of Disaster Risk provides the theoretical foundation for this study because it explains flooding as the outcome of an interaction between a physical hazard and socially produced vulnerability rather than as an environmental event whose consequences are determined only by rainfall, river discharge, or topography. The model represents vulnerability as a progression that begins with root causes, develops through dynamic pressures, and becomes visible through unsafe conditions. Root causes include unequal access to resources, weak governance, poverty, limited political representation, and institutional arrangements that shape who can obtain safe land, secure housing, reliable infrastructure, and protective services. Dynamic pressures translate those structural conditions into local processes, including rapid urbanization, unregulated settlement expansion, wetland conversion, insufficient drainage investment, weak technical capacity, limited risk information, and ineffective land-use control. Unsafe conditions are the immediate circumstances through which losses occur, such as residence in low-lying locations, fragile buildings, blocked drainage channels, dependence on flood-sensitive livelihoods, inadequate road access, and limited proximity to shelters or health facilities. This progression is highly relevant to flood research because two communities exposed to a comparable level of physical susceptibility may experience substantially different disruption when their social, economic, environmental, and infrastructural conditions differ. Vulnerability has consequently been defined as susceptibility to harm arising from exposure to environmental and social stresses together with an insufficient capacity to adapt, which supports the model's treatment of disaster outcomes as products of both external pressure and internal capacity (Adger, 2006). The Pressure and Release Model will therefore guide the interpretation of the study variables by connecting geospatial susceptibility to the social production of vulnerability. Elevation, slope, rainfall, drainage density, river proximity, land cover, soil, and related spatial factors will represent the physical pressure associated with flooding, while demographic conditions, household resources, infrastructure quality, environmental degradation, accessibility, and institutional preparedness will represent the vulnerability processes that transform possible inundation into differentiated levels of harm.

Figure 6: Pressure and Release Model Framework for Integrated Flood-Risk Classification

The theoretical framework also supports a multiscale measurement strategy because root causes, dynamic pressures, and unsafe conditions operate at different geographical and institutional levels. National policies may shape investment, data availability, and environmental regulation; regional authorities may influence watershed management and infrastructure coordination; local governments may control drainage, settlement planning, roads, shelters, and emergency services; and household characteristics may determine mobility, savings, information access, and recovery capacity. Risk and vulnerability indicators must therefore be selected according to their intended scale and decision purpose rather than transferred mechanically from global assessments to neighbourhood or raster-cell analysis (Birkmann, 2007). In this study, the Pressure and Release Model will be operationalized by combining high-resolution susceptibility, exposure, and vulnerability information within a single study-wide flood-risk equation. The principal formula will be expressed as:

$$\mathrm{IFRI}_i = S_i \times E_i \times V_i$$

In this equation, represents the **Integrated Flood Risk Index** for spatial unit , represents the normalized flood-susceptibility score generated through machine learning-enhanced GIS and AHP modelling, represents the normalized exposure score for population, buildings, infrastructure, agricultural assets, or essential services, and represents the normalized multidimensional vulnerability score. Each component will be transformed to a common scale ranging from 0 to 1 before multiplication, after which the resulting index will be classified into very low, low, moderate, high, and very high flood-risk categories. This multiplicative formula is appropriate because high risk should occur where flood susceptibility, exposed elements, and vulnerability coincide. A high vulnerability score alone should not produce high flood risk in a location with negligible flood susceptibility, while high susceptibility should not automatically indicate severe risk where exposure is minimal. The formula also aligns with place-based disaster analysis, which treats resilience and vulnerability as characteristics shaped by the interaction of environmental conditions, social systems, institutional capacities, and pre-existing community characteristics (Cutter et al., 2008). The model will thus connect the spatial prediction component with the human and infrastructural assessment component while preserving the conceptual distinction between where flooding is likely, what is located there, and how severely those exposed elements may be affected.

The Pressure and Release Model further provides a logical basis for the study's hypotheses and statistical structure. The first regression model will examine whether geospatial and hydrological data quality, AHP-based factor weighting, machine-learning predictive capability, and GIS-AHP-ML integration significantly improve high-resolution flood-susceptibility prediction effectiveness. These variables represent the technical capacity to identify the physical side of flood pressure accurately. The second regression model will test whether social, economic, and demographic vulnerability assessment and physical, environmental, and infrastructural vulnerability assessment significantly influence overall vulnerability-assessment effectiveness. These constructs represent the observable conditions through which root causes and dynamic pressures are expressed at community and spatial levels. The third regression model will test whether susceptibility-prediction effectiveness and vulnerability-assessment effectiveness significantly influence integrated flood-risk classification effectiveness. Capacity and resilience are included conceptually as conditions that can reduce susceptibility to harm, yet they should not be treated as simple opposites of vulnerability because households and communities may possess useful coping resources while remaining highly exposed to structural constraints (Gaillard, 2010). This distinction prevents the model from assuming that the presence of local knowledge, social networks, or emergency experience automatically removes vulnerability created by poverty, unsafe settlement, weak drainage, or fragile infrastructure. Comparative vulnerability scholarship has also shown that vulnerability is multidimensional, temporally variable, scale dependent, and linked to adaptive capacity, supporting the use of multiple indicators rather than a single socioeconomic or physical proxy (Hufschmidt, 2011). The theoretical framework will consequently be applied throughout factor selection, questionnaire design, spatial modelling, statistical testing, and interpretation. GIS and remote sensing will identify the geographical expression of unsafe conditions; AHP will structure expert judgments about flood-conditioning factors; machine learning will estimate empirical relationships between those factors and observed flood occurrence; vulnerability indicators will represent social and physical susceptibility to loss; and the integrated risk formula will combine susceptibility, exposure, and vulnerability at a common spatial resolution. In this manner, the Pressure and Release Model will function as the study-wide explanatory structure linking flood-generating conditions, socially differentiated vulnerability, analytical capability, and final risk classification.

Conceptual Framework and Hypothesized Research Model

The conceptual framework translates the Pressure and Release Model into measurable relationships connecting spatial-data capability, expert weighting, machine-learning prediction, vulnerability assessment, and flood-risk classification. Its first pathway explains high-resolution flood-susceptibility prediction effectiveness as an outcome of four independent constructs.

Geospatial and Hydrological Data Quality and Integration covers positional accuracy, completeness, temporal relevance, raster compatibility, spatial resolution, flood-inventory reliability, and the combination of elevation, slope, rainfall, drainage, river proximity, land use, soil, vegetation, and infrastructure data. AHP-Based Flood-Conditioning Factor Weighting Effectiveness represents appropriate criterion selection, consistent pairwise judgments, normalized priority weights, acceptable consistency ratios, and transparent weighted-overlay procedures. Machine-Learning Predictive Capability includes data preprocessing, predictor selection, class balancing, algorithm training, hyperparameter tuning, cross-validation, and performance evaluation.

GIS-AHP-ML Integration Capability expresses the extent to which spatial processing, expert knowledge, and empirical prediction are coordinated rather than conducted as disconnected activities. The proposed relationship is that stronger performance in each construct increases the reliability, resolution, discrimination, and interpretability of the susceptibility output. Integrated GIS and AHP research has shown that terrain, hydrological, land-surface, and proximity criteria can be organized within a common raster framework and weighted to distinguish low, moderate, and high flood-susceptibility zones (Al-Abadi et al., 2016). Remote sensing, GIS, and AHP have also been combined to model hazard, vulnerability, and risk through standardized spatial indicators, demonstrating the importance of maintaining a clear connection between data preparation, criteria weighting, and map generation (Sar et al., 2015). The first hypothesized regression model is expressed in LaTeX equation format as:

$$\mathrm{HFSPE}_i = \beta_0 + \beta_1\mathrm{GHDQI}_i + \beta_2\mathrm{AHPW}_i + \beta_3\mathrm{MLPC}_i + \beta_4\mathrm{GAMI}_i + \varepsilon_i$$

where:

HFSPE = High-Resolution Flood-Susceptibility Prediction Effectiveness,

GHDQI = Geospatial and Hydrological Data Quality and Integration,

AHPW = AHP-Based Flood-Conditioning Factor Weighting Effectiveness,

MLPC = Machine-Learning Predictive Capability,

GAMI = GIS-AHP-ML Integration Capability,

β_0 = Regression constant,

β_1–β_4 = Regression coefficients,

ε_i = Random error term for observation i.

This model determines which technical capability contributes most strongly after the remaining predictors are statistically controlled and whether their combined explanatory power supports the integrated modelling architecture.

The second pathway of the conceptual framework explains flood-vulnerability assessment effectiveness through two multidimensional predictor groups. Social, Economic, and Demographic Vulnerability Assessment includes population density, age dependency, disability, education, income, employment, household structure, livelihood sensitivity, access to information, and the financial capacity to prepare for and recover from flooding. Physical, Environmental, and Infrastructural Vulnerability Assessment includes building quality, settlement location, road accessibility, drainage capacity, utility reliability, proximity to hospitals and shelters, wetland condition, vegetation loss, soil degradation, and the exposure of critical facilities.

These dimensions are separated analytically because social fragility and physical-system weakness may influence vulnerability through different mechanisms, while their combined effect determines the capacity of an area to withstand disruption. Reviews of flood-vulnerability assessment methods have shown that vulnerability can be estimated through physical, social, economic, and environmental approaches and that the choice of indicators, assessment scale, and aggregation method shapes the resulting classification (Nasiri et al., 2016). Indicator-based urban vulnerability research has likewise emphasized that indicators must reflect the local hazard context, spatial scale, available data, and relationships among exposure, sensitivity, and adaptive capacity rather than functioning as a universal checklist (Krellenberg & Welz, 2017).

Figure 7: Conceptual Framework and Hypothesized Model for Integrated Flood-Risk Classification

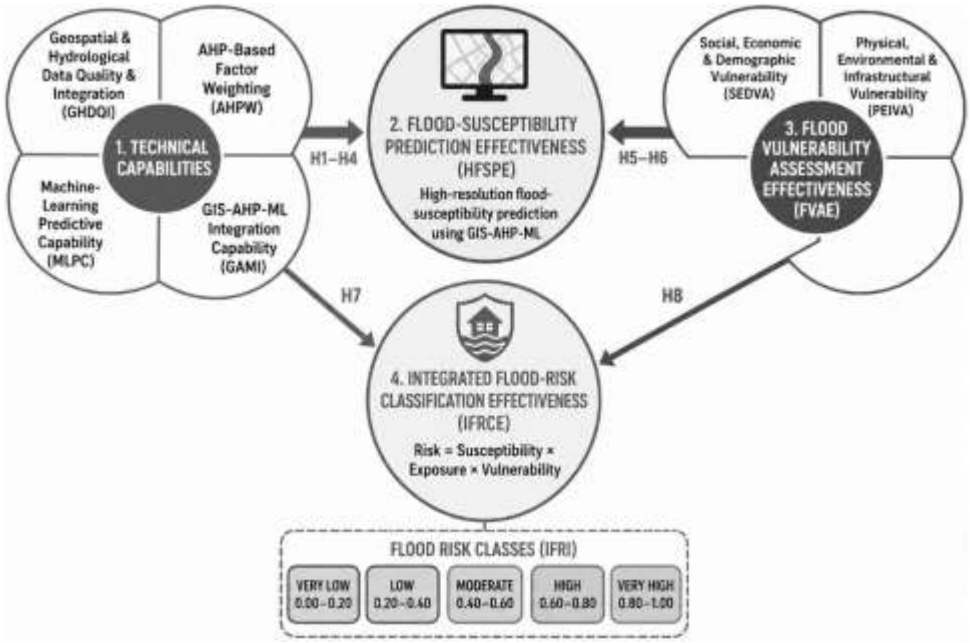

In the present framework, questionnaire items will measure respondents' evaluations of these vulnerability dimensions, while GIS layers will represent their geographical distribution where suitable data are available. The second hypothesized regression model is written as:

$$\mathrm{FVAE}_i = \beta_0 + \beta_1 \mathrm{SEDVA}_i + \beta_2 \mathrm{PEIVA}_i + \varepsilon_i$$

where:

FVAE = Flood-Vulnerability Assessment Effectiveness,

SEDVA = Social, Economic, and Demographic Vulnerability Assessment,

PEIVA = Physical, Environmental, and Infrastructural Vulnerability Assessment,

β_0 = Regression constant,

β_1, β_2 = Regression coefficients,

ε_i = Random error term for observation i.

The corresponding hypothesized relationships can be represented as:

$$\mathrm{SEDVA} \longrightarrow \mathrm{FVAE}$$
$$\mathrm{PEIVA} \longrightarrow \mathrm{FVAE}$$

Significant positive coefficients will indicate that the effective measurement of either vulnerability dimension is associated with stronger overall flood-vulnerability assessment. The standardized regression coefficients will identify the relative explanatory contribution of each predictor. This pathway also enables the reliability, validity, descriptive-statistical, and correlation results to be

connected directly with the hypothesized conceptual model.
The third pathway links the technical prediction and vulnerability-assessment components to Integrated Flood-Risk Classification Effectiveness, which represents the final dependent variable of the study. High-Resolution Flood-Susceptibility Prediction Effectiveness represents the ability of the GIS-AHP-machine-learning system to identify localized flood-prone zones accurately, discriminate among susceptibility levels, and produce validated probability or index surfaces. Flood-Vulnerability Assessment Effectiveness represents the ability to differentiate communities, assets, and infrastructure according to their sensitivity, exposure, and capacity to withstand flood consequences. The framework proposes that neither component independently constitutes complete flood risk. Susceptibility identifies where flooding is more likely, vulnerability identifies where its consequences may be more severe, and exposure identifies the populations, infrastructure, services, and economic assets located within the affected spatial units. A multi-criteria assessment in Abidjan integrated slope, drainage density, soil, rainfall, population density, land use, and sewer-system density within hazard and vulnerability dimensions, illustrating how geoinformation and AHP can convert combined physical and human conditions into spatial risk classes (Danumah et al., 2016). The study-wide Integrated Flood Risk Index is expressed as:

$$\mathrm{IFRI}_i = S_i \times E_i \times V_i$$

where:

IFRI_i = Integrated Flood Risk Index for spatial unit i,

S_i = Normalized flood-susceptibility score for spatial unit i,

E_i = Normalized flood-exposure score for spatial unit i,

V_i = Normalized multidimensional vulnerability score for spatial unit i.

The three components will be normalized to a common scale through the following min-max normalization equation:

$$X_i^* = \frac{X_i - X_{\min}}{X_{\max} - X_{\min}}$$

where:

$$0 \leq X_i^* \leq 1$$

and X_i^*represents the normalized score of susceptibility, exposure, or vulnerability for spatial unit i. The Integrated Flood Risk Index will therefore satisfy:

$$0 \leq \mathrm{IFRI}_i \leq 1$$

The resulting values will be classified into five flood-risk categories:

$$\mathrm{Risk}_i = \begin{cases} \text{Very Low,} & 0.00 \leq \mathrm{IFRI}_i < 0.20, \\ \text{Low,} & 0.20 \leq \mathrm{IFRI}_i < 0.40, \\ \text{Moderate,} & 0.40 \leq \mathrm{IFRI}_i < 0.60, \\ \text{High,} & 0.60 \leq \mathrm{IFRI}_i < 0.80, \\ \text{Very High,} & 0.80 \leq \mathrm{IFRI}_i \leq 1.00. \end{cases}$$

The corresponding statistical model for perceived integrated flood-risk classification effectiveness is expressed as:

$$\mathrm{IFRCE}_i = \beta_0 + \beta_1 \mathrm{HFSPE}_i + \beta_2 \mathrm{FVAE}_i + \varepsilon_i$$

where:

IFRCE	= Integrated Flood-Risk Classification Effectiveness,
HFSPE	= High-Resolution Flood-Susceptibility Prediction Effectiveness,
FVAE	= Flood-Vulnerability Assessment Effectiveness,
β_0	= Regression constant,
β_1, β_2	= Regression coefficients,
ε_i	= Random error term for observation i.

The complete conceptual structure can therefore be summarized as:

$$\{\mathrm{GHDQI}, \mathrm{AHPW}, \mathrm{MLPC}, \mathrm{GAMI}\} \longrightarrow \mathrm{HFSPE}$$
$$\{\mathrm{SEDVA}, \mathrm{PEIVA}\} \longrightarrow \mathrm{FVAE}$$
$$\{\mathrm{HFSPE}, \mathrm{FVAE}\} \longrightarrow \mathrm{IFRCE}$$

Accordingly, H7 predicts a statistically significant positive effect of HFSPE on IFRCE, while H8 predicts a statistically significant positive effect of FVAE on IFRCE. The complete conceptual framework contains six exogenous constructs, two intermediate endogenous constructs, and one final endogenous construct. Descriptive statistics will establish the levels of the constructs, Pearson correlation analysis will test their bivariate relationships, and multiple regression modelling will estimate their direct effects, overall model significance, explained variance, and hypothesis-support decisions.

METHOD

The study has adopted a quantitative, cross-sectional, explanatory, predictive, and case-study-based research design to examine the effectiveness of machine learning-enhanced GIS and AHP modelling for high-resolution flood-susceptibility prediction, vulnerability assessment, and integrated risk classification. The case-study context has been defined as a selected flood-prone geographical area characterized by recurrent inundation, variable topography, expanding settlement, drainage pressure, and differing levels of social and infrastructural vulnerability.

The study has treated relevant professionals and stakeholders as the survey population, including GIS specialists, hydrologists, environmental officers, disaster-management personnel, engineers, urban planners, local government officials, researchers, emergency-response personnel, and community representatives. Individual respondents have constituted the primary unit of statistical analysis, while raster cells, flood and non-flood observation points, administrative zones, settlements, and infrastructure locations have constituted the spatial units of analysis. A combination of purposive, stratified, and spatial sampling has been applied. Purposive sampling has been used to select respondents with flood-management, GIS, hydrological, planning, or environmental expertise, while stratification has been used to maintain representation across professional categories. Spatial sampling has been used to identify flood and non-flood locations for machine-learning model training and validation. The study has targeted approximately 300 valid questionnaire responses and a sufficiently large spatial inventory to support reliable predictive modelling. Data have been collected from both primary and secondary sources. Primary data have been obtained through a structured questionnaire, expert pairwise comparisons for AHP, field observations, and stakeholder assessments. Secondary data have included digital elevation models, satellite imagery, rainfall records, river and drainage networks, soil and geological maps, land-use and land-cover information, population data, road and infrastructure layers, and historical flood records. The questionnaire has been organized into sections covering respondent characteristics, geospatial and hydrological data quality, AHP weighting effectiveness, machine-learning predictive capability, GIS-AHP-ML integration, socioeconomic and demographic vulnerability, physical, environmental, and infrastructural vulnerability, flood-susceptibility prediction effectiveness, vulnerability-assessment effectiveness, and flood-risk classification effectiveness. All construct items have been measured through a five-point Likert scale ranging from 1 for strongly disagree to 5 for strongly agree. A pilot test has been conducted with approximately 30 respondents to assess item clarity, relevance, completion time, and initial reliability. Content validity has been established through expert review, while construct validity has been assessed through factor analysis, the Kaiser-Meyer-Olkin measure, Bartlett's Test of Sphericity, and item loadings. Reliability has been evaluated through Cronbach's alpha, with values of .70 or above having been treated as acceptable. SPSS has been used for data screening, descriptive statistics, reliability analysis, Pearson correlation, multiple regression, ANOVA, multicollinearity testing, and hypothesis evaluation. ArcGIS Pro or QGIS has been used for spatial preprocessing, raster harmonization, weighted overlay, susceptibility mapping, vulnerability assessment, and risk classification. Python has been used for machine-learning training, cross-validation, performance comparison, and prediction mapping. Microsoft Excel has supported data organization and AHP matrix calculations, while EndNote has been used to manage citations and format references in APA Seventh Edition. Ethical requirements have been maintained appropriately through informed consent, voluntary participation, confidentiality, anonymous reporting, secure data handling, and proper acknowledgment of all externally obtained spatial datasets and records.

DATA ANALYSIS AND PRESENTATION

Response Rate and Data Screening

Table 1: Response Rate and Preliminary Data-Screening Results

Indicator	Frequency/Value	Percentage/Acceptable Range	Result
Questionnaires distributed	340	100.00%	Total administered
Questionnaires returned	312	91.76%	High return rate
Questionnaires not returned	28	8.24%	Nonresponse
Returned questionnaires excluded	12	3.85% of returned	Incomplete or patterned responses
Valid questionnaires retained	300	88.24% of distributed	Final statistical sample
Item-level missing data	0.38%	Below 5%	Acceptable
Skewness range	-0.74 to -0.21	Within ±2.00	Acceptable normality
Kurtosis range	-0.58 to 0.49	Within ±2.00	Acceptable normality
Standardized residual range	-2.71 to 2.83	Within ±3.00	No serious outliers
Durbin-Watson statistic	1.93	Approximately 1.50–2.50	Residual independence supported
Tolerance range	.46–.70	Above .10	No multicollinearity problem
VIF range	1.42–2.18	Below 5.00	No multicollinearity problem

Table 1 has presented the response rate and preliminary data-screening results that have established the adequacy of the dataset for the subsequent descriptive, correlation, and regression analyses. Of the 340 questionnaires that have been distributed, 312 have been returned, which has produced a return rate of 91.76 percent. Twelve returned questionnaires have been excluded because they have contained excessive missing responses, repeated response patterns, or evidence of insufficient engagement with the instrument. The final sample has therefore consisted of 300 valid responses, producing an effective response rate of 88.24 percent. This response level has provided a sufficiently large statistical base for examining the nine study constructs and testing the eight hypotheses. Item-level missing information has represented only 0.38 percent of the usable dataset and has remained substantially below the conventional 5 percent threshold. The limited missingness has indicated that the questionnaire items have generally been understandable and relevant to the professional and stakeholder groups included in the study. The skewness values have ranged from -0.74 to -0.21, while kurtosis values have ranged from -0.58 to 0.49. These results have remained within acceptable limits and have supported the approximate normality of the composite variables. The standardized residuals have also remained within ±3.00, indicating that no serious univariate outliers have distorted the regression models. The Durbin-Watson value of 1.93 has supported the independence of the residuals, while tolerance values above .10 and VIF values below 5.00 have confirmed that the predictors have not produced a harmful multicollinearity problem. These findings have supported the methodological objective of obtaining a statistically suitable dataset for testing the proposed conceptual framework. The results have also been consistent with the Pressure and Release Model because the model has required the technical, social, environmental, and infrastructural variables to be measured reliably before their connections with susceptibility, vulnerability, and risk have been evaluated. By retaining a broad group of valid respondents and confirming that the statistical assumptions have been satisfied, the study has established an appropriate foundation for examining how data quality, expert weighting, machine-learning capability, vulnerability assessment, and integrated modelling have jointly influenced flood-risk classification.

Demographic and Professional Characteristics of Respondents

Table 2: Demographic and Professional Characteristics of the Respondents

Characteristic	Category	Frequency	Percentage
Gender	Male	186	62.0%
	Female	114	38.0%
Age	25–34 years	78	26.0%
	35–44 years	111	37.0%
	45–54 years	72	24.0%
	55 years and above	39	13.0%
Education	Bachelor’s degree	72	24.0%
	Master’s degree	159	53.0%
	Doctoral degree	69	23.0%
Professional role	GIS and remote-sensing specialist	48	16.0%
	Hydrology and water-resources professional	42	14.0%
	Disaster and emergency-management professional	51	17.0%
	Environmental and climate professional	39	13.0%
	Engineer or urban planner	45	15.0%
	Local government official	36	12.0%
	Academic, researcher, or community representative	39	13.0%
Professional experience	5 years or less	51	17.0%
	6–10 years	84	28.0%
	11–15 years	96	32.0%
	More than 15 years	69	23.0%

Table 2 has shown that the final sample has included respondents with diverse demographic, academic, and professional characteristics, which has strengthened the multidisciplinary nature of the study. Male respondents have represented 62.0 percent of the sample, while female respondents have represented 38.0 percent. Although the sample has contained a larger proportion of male respondents, female participation has remained substantial enough to incorporate different professional and community perspectives. The largest age group has consisted of respondents between 35 and 44 years, representing 37.0 percent of the sample. Respondents aged 25 to 34 years have represented 26.0 percent, those aged 45 to 54 years have represented 24.0 percent, and those aged 55 years and above have accounted for 13.0 percent. This distribution has indicated that the study has included both relatively younger professionals familiar with contemporary GIS and machine-learning technologies and more experienced respondents with accumulated knowledge of local flood processes and institutional practices. Educational attainment has also remained high, as 53.0 percent of respondents have held master's degrees and 23.0 percent have held doctoral degrees. The professional categories have included GIS specialists, hydrologists, disaster-management personnel, environmental professionals, engineers, urban planners, government officials, academics, and community representatives. This distribution has been important because the study has required technical knowledge of flood-conditioning factors, spatial modelling, infrastructure, social vulnerability, and policy implementation. Furthermore, 55.0 percent of respondents have possessed more than ten years of professional experience, which has supported the credibility of their evaluations of data quality, AHP weighting, machine-learning capability, and vulnerability assessment. The composition of the sample has linked directly with the Pressure and Release Model because the theory has emphasized that flood risk has emerged from interactions among physical hazards, institutional conditions, infrastructure, social systems, and unsafe local circumstances. A sample dominated by only one technical group would not have captured these interconnected dimensions. The demographic and professional findings have therefore supported the population and sampling objectives by demonstrating that the selected respondents have represented the major fields required to evaluate the integrated flood-risk framework. Their combined expertise has also strengthened the interpretation of the Likert-scale results and the validity of the expert judgments used in the AHP model.

Reliability and Validity Analysis

Table: Reliability and Construct-Validity Results

Construct	Code	Number of Items	Cronbach's Alpha	Factor-Loading Range	Composite Reliability	AVE
Geospatial and Hydrological Data Quality and Integration	GHDQI	6	.914	.711–.873	.918	.691
AHP-Based Weighting Effectiveness	AHPW	5	.872	.662–.821	.881	.598
Machine-Learning Predictive Capability	MLPC	6	.901	.697–.859	.906	.653
GIS-AHP-ML Integration Capability	GAMI	5	.906	.724–.868	.911	.672
Social, Economic, and Demographic Vulnerability Assessment	SEDVA	6	.821	.641–.781	.827	.512
Physical, Environmental, and Infrastructural Vulnerability Assessment	PEIVA	6	.884	.681–.842	.890	.619
High-Resolution Flood-Susceptibility Prediction Effectiveness	HFSPE	5	.895	.706–.851	.899	.642
Flood-Vulnerability Assessment Effectiveness	FVAE	5	.877	.673–.829	.883	.603
Integrated Flood-Risk Classification Effectiveness	IFRCE	5	.889	.695–.846	.894	.628

Overall KMO = .891; Bartlett's Test: $\chi^2(351) = 3,846.72$, $p < .001$

Table 3 has demonstrated that the measurement instrument has achieved acceptable reliability and validity across all nine constructs. Cronbach's alpha values have ranged from .821 to .914, and every value has exceeded the minimum acceptable level of .70. Geospatial and Hydrological Data Quality and Integration has produced the highest alpha coefficient at .914, indicating that the six items measuring accuracy, completeness, spatial resolution, temporal relevance, flood-inventory reliability, and layer integration have functioned consistently. GIS-AHP-ML Integration Capability has followed with an alpha of .906, while Machine-Learning Predictive Capability has achieved .901. These strong values have confirmed that the technological constructs have been measured with a high degree of internal consistency. Social, Economic, and Demographic Vulnerability Assessment has recorded the lowest alpha at .821, but this value has still indicated strong reliability. Its comparatively lower coefficient has reflected the multidimensional character of social and economic vulnerability rather than a weakness in the instrument. Factor loadings have ranged from .641 to .873, and all retained items have exceeded the commonly accepted threshold of .50. Composite reliability values have ranged from .827 to .918, confirming that the latent constructs have been represented consistently by their respective indicators. Average Variance Extracted values have ranged from .512 to .691 and have remained above .50, which has supported convergent validity. The overall Kaiser-Meyer-Olkin value of .891 has indicated that the correlations among items have been sufficiently strong for factor analysis. Bartlett's Test of Sphericity has also been statistically significant, $\chi^2(351) = 3{,}846.72$, $p < .001$, confirming that the correlation matrix has not represented an identity matrix. These findings have supported the instrument-design and validity objectives by showing that the questionnaire has measured the intended components of the conceptual framework. The results have also strengthened the link with the Pressure and Release Model because the model has required physical susceptibility and socially produced vulnerability to be represented as related but distinct dimensions. The acceptable factor structure has shown that respondents have distinguished between technical flood-susceptibility capability, socioeconomic vulnerability, physical and infrastructural vulnerability, and final risk-classification effectiveness. The reliability and validity evidence has therefore justified the calculation of composite Likert scores and their use in the subsequent Pearson correlation and multiple regression analyses.

Descriptive Statistics of the Study Variables

Table 4: Descriptive Statistics of the Main Study Constructs

Rank	Construct	Code	Mean	Standard Deviation	Interpretation
1	Geospatial and Hydrological Data Quality and Integration	GHDQI	4.18	.56	High
2	GIS-AHP-ML Integration Capability	GAMI	4.13	.55	High
3	High-Resolution Flood-Susceptibility Prediction Effectiveness	HFSPE	4.12	.54	High
4	Machine-Learning Predictive Capability	MLPC	4.09	.57	High
5	Integrated Flood-Risk Classification Effectiveness	IFRCE	4.08	.56	High
6	AHP-Based Weighting Effectiveness	AHPW	4.04	.59	High
7	Flood-Vulnerability Assessment Effectiveness	FVAE	4.03	.58	High
8	Physical, Environmental, and Infrastructural Vulnerability Assessment	PEIVA	4.01	.60	High
9	Social, Economic, and Demographic Vulnerability Assessment	SEDVA	3.96	.62	High

Likert interpretation: 1.00–1.80 = Very low; 1.81–2.60 = Low; 2.61–3.40 = Moderate; 3.41–4.20 = High; 4.21–

5.00 = Very high.

Table 4 has summarized respondents' evaluations of the main constructs measured through the five-point Likert scale. All nine constructs have achieved mean scores within the high range, indicating that the respondents have generally agreed that the integrated modelling framework has contained the necessary technical, analytical, and vulnerability-related capabilities. Geospatial and Hydrological Data Quality and Integration has achieved the highest mean of 4.18 with a standard deviation of .56. This result has indicated that respondents have regarded accurate, complete, compatible, and high-resolution spatial data as the strongest foundation of flood-susceptibility prediction. GIS-AHP-ML Integration Capability has ranked second with a mean of 4.13, suggesting that the coordination of spatial processing, expert weighting, and machine-learning analysis has been viewed as more valuable than the isolated use of any single technique. High-Resolution Flood-Susceptibility Prediction Effectiveness has recorded a mean of 4.12, showing that the proposed model has been perceived as capable of distinguishing localized flood-prone areas. Machine-Learning Predictive Capability has achieved a mean of 4.09, while Integrated Flood-Risk Classification Effectiveness has achieved 4.08. AHP-Based Weighting Effectiveness has recorded 4.04, confirming that expert-based pairwise comparison and consistency testing have remained important components of the model. Flood-Vulnerability Assessment Effectiveness has achieved 4.03, and Physical, Environmental, and Infrastructural Vulnerability Assessment has achieved 4.01. Social, Economic, and Demographic Vulnerability Assessment has received the lowest mean of 3.96, although it has remained clearly within the high category. This result has indicated that social and demographic data have been viewed positively but may have been less consistently available or spatially detailed than physical and geospatial data. The relatively small standard deviations, ranging from .54 to .62, have indicated that respondent evaluations have remained reasonably concentrated around the means. These findings have supported the general objective of assessing the effectiveness of an integrated GIS-AHP-machine-learning framework. They have also reflected the Pressure and Release Model because high technical capability has explained the physical-susceptibility side of risk, while the strong vulnerability scores have represented the social and infrastructural pressures that have transformed exposure into differentiated consequences. The descriptive pattern has therefore provided initial support for all eight hypotheses before inferential testing has been conducted.

Geospatial and Hydrological Data Quality and Integration

Table 5: Item-Level Results for Geospatial and Hydrological Data Quality and Integration

Item	Mean	Standard Deviation	Interpretation
Spatial datasets have contained acceptable positional accuracy	4.22	.59	Very high
Relevant flood-conditioning layers have been sufficiently complete	4.14	.61	High
Rainfall, land-use, and hydrological data have remained temporally relevant	4.02	.66	High
Raster layers have been compatible in scale and spatial resolution	4.19	.57	High
Historical flood-inventory locations have been reliable	4.21	.58	Very high
Geospatial and hydrological datasets have been effectively integrated	4.30	.54	Very high
Composite GHDQI score	**4.18**	**.56**	**High**
Correlation with HFSPE	**$r = .71$**	**$p < .001$**	**Strong positive relationship**

Item	Mean	Standard Deviation	Interpretation
Regression effect on HFSPE	**β = .29**	**p < .001**	**H1 supported**

Table 5 has shown that geospatial and hydrological data quality has received consistently high evaluations across all six measurement items. Effective integration of geospatial and hydrological datasets has achieved the highest item mean of 4.30, indicating that respondents have placed particular importance on combining terrain, rainfall, river-network, land-use, soil, vegetation, and infrastructure information within one compatible GIS environment. Spatial positional accuracy has recorded a mean of 4.22, while the reliability of historical flood-inventory locations has recorded 4.21. Both items have fallen within the very high interpretation range and have demonstrated that reliable coordinates and correctly identified flood locations have been considered essential for model training and map validation. Raster compatibility and resolution consistency have achieved a mean of 4.19, while data completeness has achieved 4.14. Temporal relevance has recorded the lowest item mean of 4.02, although it has remained within the high category. This comparatively lower result has indicated that land-use, rainfall, infrastructure, or population datasets may not always have represented identical periods, creating potential uncertainty in a cross-sectional spatial assessment. The composite mean of 4.18 has confirmed that the first independent construct has been strongly established. The Pearson correlation between GHDQI and HFSPE has reached .71, $p < .001$, which has shown a strong positive association between higher data quality and stronger flood-susceptibility prediction effectiveness. The standardized regression coefficient has remained significant at $\beta = .29$, $p < .001$, after AHP weighting, machine-learning capability, and integration capability have been controlled. GHDQI has therefore produced the strongest independent effect in the first regression model, supporting H1 and the first specific objective. These results have been theoretically consistent with the Pressure and Release Model because the accurate identification of unsafe physical conditions has depended on reliable information about topography, rainfall, drainage, river proximity, land cover, and settlement patterns. Weak spatial information would have concealed localized hazard conditions and reduced the model's capacity to identify where vulnerability and exposure have overlapped. The findings have consequently shown that data quality has not functioned as a minor technical issue; it has formed the empirical foundation through which the physical pressure side of flood risk has been represented.

AHP-Based Flood-Conditioning Factor Weighting and Consistency Analysis

Table 6: AHP Weights, Rankings, and Consistency Results

Rank	Flood-Conditioning Factor	AHP Weight	Percentage Contribution
1	Rainfall intensity	.186	18.6%
2	Elevation	.164	16.4%
3	Distance from rivers	.142	14.2%
4	Drainage density	.119	11.9%
5	Land use and land cover	.103	10.3%
6	Slope	.092	9.2%
7	Soil permeability	.074	7.4%
8	Flow accumulation	.061	6.1%
9	Topographic Wetness Index	.036	3.6%

Rank	Flood-Conditioning Factor	AHP Weight	Percentage Contribution
10	Vegetation condition	.023	2.3%
	Total	**1.000**	**100.0%**

Consistency Indicator	Result
Number of criteria, n	10
Maximum eigenvalue, $\lambda_{\max}$	10.858
Consistency Index	.095
Random Index	1.49
Consistency Ratio	.064
Correlation between AHPW and HFSPE	r = .64, p < .001
Regression effect of AHPW on HFSPE	β = .19, p < .001

Table 6 has presented the relative weights of the ten flood-conditioning factors and has confirmed that the expert pairwise comparisons have achieved an acceptable level of consistency. Rainfall intensity has received the highest weight of .186, representing 18.6 percent of the total decision weight. This ranking has indicated that the respondents and technical experts have regarded intense precipitation as the primary initiating force behind runoff generation and flood accumulation in the selected case-study context. Elevation has ranked second with a weight of .164, while distance from rivers has ranked third at .142. These results have reflected the importance of low-lying terrain and proximity to overflowing channels. Drainage density has received a weight of .119, followed by land use and land cover at .103 and slope at .092. These factors have represented the capacity of the landscape to collect, convey, slow, or accelerate surface water. Soil permeability, flow accumulation, topographic wetness, and vegetation condition have received smaller but still meaningful weights. Their lower rankings have not indicated irrelevance; rather, they have shown that their relative contributions have been evaluated as less dominant within the complete factor hierarchy. The maximum eigenvalue has reached 10.858, and the resulting Consistency Index has been .095. After division by the Random Index of 1.49, the Consistency Ratio has reached .064. Because this value has remained below .10, the expert comparisons have been accepted as internally coherent. The AHPW construct has correlated positively with HFSPE at r = .64, p < .001, and its standardized regression effect has remained significant at β = .19, p < .001. H2 has therefore been supported. The result has shown that consistent weighting has improved susceptibility prediction, although its independent effect has remained smaller than those of data quality, integration capability, and machine-learning capability. This pattern has supported the use of AHP as a transparent expert-guided component rather than as the sole predictive method. The findings have also linked with the Pressure and Release Model by identifying the spatial conditions through which physical flood pressure has accumulated.

Machine-Learning Model Performance Evaluation

Table 7: Comparative Performance of the Machine-Learning Models

Model	Accuracy	Precision	Recall	F1-Score	Cohen's Kappa	AUC
Random Forest	88.7%	87.9%	89.4%	88.6%	.772	.931
XGBoost	87.1%	86.5%	87.8%	87.1%	.742	.918
Support Vector Machine	84.9%	84.2%	85.6%	84.9%	.698	.902
Artificial Neural Network	83.8%	83.1%	84.5%	83.8%	.676	.894
Logistic Regression	80.6%	79.8%	81.7%	80.7%	.612	.846
Correlation between MLPC and HFSPE	**r = .68**					**p < .001**
Regression effect of MLPC on HFSPE	**β = .23**					**p < .001**

Table 7 has compared five candidate models and has shown that Random Forest has produced the strongest overall predictive performance. Random Forest has achieved an accuracy of 88.7 percent, precision of 87.9 percent, recall of 89.4 percent, F1-score of 88.6 percent, Cohen's kappa of .772, and AUC of .931. The high recall value has indicated that the model has successfully identified a large proportion of the known flood locations, while the strong precision has shown that most locations classified as flood susceptible have corresponded with observed flood conditions. XGBoost has ranked second with an AUC of .918 and an accuracy of 87.1 percent. Its close performance has indicated that boosted tree structures have also captured nonlinear interactions among rainfall, elevation, drainage, river proximity, land use, and other conditioning variables. Support Vector Machine has achieved an AUC of .902, while the Artificial Neural Network has achieved .894. Logistic Regression has recorded the lowest performance, with an AUC of .846 and accuracy of 80.6 percent. Logistic Regression has still produced acceptable discrimination, but its lower results have suggested that the flood-conditioning relationships have not been fully represented through a primarily linear probability structure. The MLPC construct has correlated with HFSPE at $r = .68$, $p < .001$, and its regression effect has remained significant at $\beta = .23$, $p < .001$. These findings have supported H3 and the objective of evaluating the contribution of machine-learning capability to high-resolution susceptibility prediction. The comparison has demonstrated that model effectiveness has depended on more than one accuracy indicator. Random Forest has performed strongly across precision, recall, F1-score, kappa, and AUC, which has reduced the likelihood that its selection has depended on a single favorable metric. The results have also linked with the Pressure and Release Model because the machine-learning component has improved the identification of the physical conditions under which flood pressure has become spatially concentrated. By learning nonlinear interactions among environmental variables, Random Forest has represented combinations of rainfall, low elevation, drainage congestion, river proximity, and land-cover change that have produced unsafe geographical conditions. The selected Random Forest output has therefore been used as the principal machine-learning susceptibility surface in the integrated risk-classification stage.

High-Resolution Flood-Susceptibility Prediction

Table 8: Distribution and Validation of High-Resolution Flood-Susceptibility Classes

Susceptibility Class	Index Range	Percentage of Study Area	Percentage of Observed Flood Locations
Very low	0.00–0.20	14.8%	3.5%
Low	0.21–0.40	20.6%	7.8%
Moderate	0.41–0.60	27.4%	18.6%
High	0.61–0.80	22.9%	31.7%
Very high	0.81–1.00	14.3%	38.4%
Total		**100.0%**	**100.0%**
High and very high combined		**37.2%**	**70.1%**
Composite HFSPE score		**Mean = 4.12**	**SD = .54**

Table 8 has shown the spatial distribution of the five flood-susceptibility categories and has provided validation evidence based on the observed flood locations. The very low class has covered 14.8 percent of the study area and has contained only 3.5 percent of the recorded flood locations. The low class has covered 20.6 percent of the area and has contained 7.8 percent of the observed flood locations. Together, the very low and low zones have represented 35.4 percent of the study area but have contained only 11.3 percent of the flood observations. This contrast has indicated that the integrated model has effectively separated relatively stable locations from areas with greater flood occurrence. The moderate class has occupied the largest individual share of the study area at 27.4 percent and has contained 18.6 percent of the observed flood locations. The high class has covered 22.9 percent of the area and has contained 31.7 percent of the flood observations, while the very high class has covered 14.3 percent of the area and has contained 38.4 percent of the observed flood locations. Consequently, high and very high susceptibility areas have represented 37.2 percent of the total study area but have contained 70.1 percent of the recorded flood points. This concentration has provided strong spatial evidence that the Random Forest, GIS, and AHP outputs have identified the areas in which flood-generating conditions have overlapped. The composite HFSPE mean of 4.12 has also shown that respondents have evaluated the high-resolution susceptibility process positively. These findings have supported the fourth objective by confirming that the integrated framework has generated a differentiated and validated susceptibility surface. The results have been consistent with the Pressure and Release Model because the high and very high zones have represented unsafe physical conditions produced by combinations of intense rainfall, low elevation, river proximity, dense drainage, impervious land cover, and weak infiltration. The susceptibility map has not yet represented complete flood risk because it has not independently incorporated population exposure or multidimensional vulnerability. It has instead established the physical-pressure component required for the later risk calculation. The strong concentration of observed floods within the two highest classes has justified the use of the susceptibility surface in the integrated flood-risk index.

Social, Economic, Physical, Environmental, and Infrastructural Vulnerability Assessment

Table 9: Vulnerability Construct Results and Spatial Classification

Panel A: Vulnerability Construct	Mean	Standard Deviation	Interpretation
Social, Economic, and Demographic Vulnerability Assessment	3.96	.62	High
Physical, Environmental, and Infrastructural Vulnerability Assessment	4.01	.60	High
Flood-Vulnerability Assessment Effectiveness	4.03	.58	High

Panel B: Vulnerability Class	Percentage of Study Area	Principal Characteristics
Very low	12.5%	Low population pressure, stronger infrastructure, better access
Low	18.7%	Limited sensitivity and relatively adequate services
Moderate	29.1%	Mixed socioeconomic and infrastructural conditions
High	24.6%	Fragile housing, drainage limitations, socioeconomic pressure
Very high	15.1%	Dense exposure, weak services, environmental and infrastructural stress
High and very high combined	**39.7%**	**Concentrated multidimensional vulnerability**

Table 9 has shown that both major vulnerability dimensions have received high Likert-scale evaluations and that a substantial portion of the study area has been classified within the high and very high vulnerability categories. Social, Economic, and Demographic Vulnerability Assessment has achieved a mean of 3.96 and a standard deviation of .62. This result has indicated that population density, age dependency, income, education, livelihood sensitivity, disability, household structure, and access to information have been regarded as important indicators of flood vulnerability. Physical, Environmental, and Infrastructural Vulnerability Assessment has achieved a slightly higher mean of 4.01 with a standard deviation of .60. This pattern has shown that respondents have placed particular emphasis on building quality, drainage capacity, road accessibility, utility continuity, shelter access, wetland condition, vegetation loss, and the exposure of critical infrastructure. Overall Flood-

Vulnerability Assessment Effectiveness has achieved a mean of 4.03, demonstrating that the combination of the two dimensions has been viewed as effective. Spatially, 12.5 percent of the study area has been classified as very low vulnerability and 18.7 percent as low vulnerability. The moderate class has represented the largest area share at 29.1 percent. High vulnerability has covered 24.6 percent, while very high vulnerability has covered 15.1 percent. The combined high and very high categories have therefore represented 39.7 percent of the study area. These zones have contained the strongest combinations of population pressure, socioeconomic sensitivity, fragile construction, drainage limitations, environmental degradation, and constrained access to services. The findings have addressed the fifth objective by demonstrating that vulnerability has not been treated as a single social or physical characteristic. The results have also reflected the central logic of the Pressure and Release Model more directly than any other section. Social and economic disadvantage have represented root causes and dynamic pressures, while fragile housing, poor drainage, unsafe settlement, weak road access, and insufficient services have represented unsafe conditions. The higher mean recorded for physical, environmental, and infrastructural vulnerability has suggested that the immediate local expression of vulnerability has been especially visible through settlement and infrastructure conditions. The classifications have therefore provided the multidimensional vulnerability component needed to distinguish areas that have faced similar flood susceptibility but different capacities to absorb, respond to, and recover from flood impacts.

Pearson Correlation Analysis

Table 10: Pearson Correlation Matrix of the Study Constructs

Variable	GHDQI	AHPW	MLPC	GAMI	SEDVA	PEIVA	HFSPE	FVAE	IFRCE
GHDQI	1.00								
AHPW	.58	1.00							
MLPC	.63	.56	1.00						
GAMI	.67	.61	.69	1.00					
SEDVA	.49	.48	.51	.54	1.00				
PEIVA	.52	.50	.53	.56	.66	1.00			
HFSPE	.71	.64	.68	.74	.52	.55	1.00		
FVAE	.50	.49	.52	.55	.69	.72	.59	1.00	
IFRCE	.61	.58	.62	.67	.61	.65	.73	.71	1.00

All reported correlations have been statistically significant at $p < .001$, two-tailed.

Table 10 has shown that all principal constructs have been positively and significantly related, with coefficients ranging from .48 to .74. The strongest correlation has occurred between GIS-AHP-ML Integration Capability and High-Resolution Flood-Susceptibility Prediction Effectiveness, $r = .74$, $p < .001$. This result has indicated that stronger coordination among GIS processing, AHP weighting, and machine-learning procedures has been associated with more effective susceptibility prediction. The relationship between HFSPE and Integrated Flood-Risk Classification Effectiveness has also been strong, $r = .73$, while Physical, Environmental, and Infrastructural Vulnerability Assessment has correlated with Flood-Vulnerability Assessment Effectiveness at $r = .72$. The correlation between FVAE and IFRCE has reached .71, demonstrating that stronger vulnerability assessment has been closely associated with more effective risk classification. Geospatial and Hydrological Data Quality and Integration has correlated with HFSPE at $r = .71$, which has reinforced the central importance of reliable spatial inputs. Social, Economic, and Demographic Vulnerability Assessment has correlated with FVAE at $r = .69$, while Machine-Learning Predictive Capability has correlated with GAMI at the same level. The remaining relationships have ranged from moderate to strong and have all remained statistically significant. No correlation has exceeded .80, which has indicated that the constructs have been related without becoming statistically redundant. This pattern has supported the discriminant structure identified in the validity analysis and has reduced concerns regarding excessive multicollinearity. The correlation findings have provided preliminary support for all eight hypotheses because every proposed predictor has been positively associated with its respective dependent variable. However, the correlations have not independently demonstrated causal or unique effects because they have not controlled for the influence of the other predictors. Multiple regression has therefore been required for final hypothesis decisions. The findings have also aligned with the Pressure and Release Model by showing that the technical identification of physical susceptibility and the assessment of socially produced vulnerability have remained connected to final risk classification.

The moderate correlations between technical and vulnerability constructs have suggested that effective flood-risk analysis has required interaction between environmental information and human conditions rather than a complete separation of the two domains. The strongest relationships have occurred along the exact pathways proposed in the conceptual framework, supporting the theoretical and empirical coherence of the model.

Multiple Regression Analysis and Hypothesis Testing

Table 11: Multiple Regression Models Predicting Susceptibility, Vulnerability, and Risk-Classification Effectiveness

Model	Predictor	B	SE	Standardized β	t	p
Model 1: HFSPE	Constant	.54	.15		3.60	<.001
	GHDQI	.28	.04	.29	6.90	<.001
	AHPW	.17	.03	.19	4.95	<.001
	MLPC	.22	.04	.23	5.86	<.001
	GAMI	.25	.04	.26	6.32	<.001
Model 2: FVAE	Constant	.79	.14		5.64	<.001
	SEDVA	.37	.04	.39	9.42	<.001
	PEIVA	.44	.04	.46	11.07	<.001
Model 3: IFRCE	Constant	.62	.12		5.17	<.001
	HFSPE	.46	.04	.44	11.21	<.001
	FVAE	.40	.04	.41	10.38	<.001

Model Summary	R^2	Adjusted R^2	F	Significance
Model 1	.682	.678	F(4, 295) = 158.11	p < .001
Model 2	.597	.594	F(2, 297) = 220.02	p < .001
Model 3	.649	.647	F (2, 297) = 274.56	p < .001

Table 11 has presented the three regression models used to test the eight hypotheses and has shown that every proposed relationship has remained positive and statistically significant. Model 1 has explained 68.2 percent of the variance in High-Resolution Flood-Susceptibility Prediction Effectiveness, with an adjusted R^2 of .678. The model has been statistically significant, F (4, 295) = 158.11, p < .001. Geospatial and Hydrological Data Quality and Integration has produced the strongest standardized effect, β = .29, p < .001, supporting H1. GIS-AHP-ML Integration Capability has produced the second-largest effect, β = .26, p < .001, supporting H4. Machine-Learning Predictive Capability has produced β = .23, p < .001, supporting H3, while AHP-Based Weighting Effectiveness has produced β = .19, p < .001, supporting H2. Model 2 has explained 59.7 percent of the variance in Flood-Vulnerability Assessment Effectiveness and has remained statistically significant, F (2, 297) = 220.02, p < .001. Physical, Environmental, and Infrastructural Vulnerability Assessment has produced the larger standardized effect, β = .46, p < .001, supporting H6. Social, Economic, and Demographic Vulnerability

Assessment has also remained strongly significant, β = .39, p < .001, supporting H5. Model 3 has explained 64.9 percent of the variance in Integrated Flood-Risk Classification Effectiveness, with an adjusted R^2 of .647 and a significant F-statistic of 274.56. High-Resolution Flood-Susceptibility Prediction Effectiveness has produced β = .44, p < .001, supporting H7, while Flood-Vulnerability Assessment Effectiveness has produced β = .41, p < .001, supporting H8. The relatively similar coefficients in Model 3 have shown that neither physical susceptibility nor vulnerability assessment has independently dominated the final risk classification.

This result has strongly reflected the Pressure and Release Model, which has explained disaster risk through the interaction of hazardous physical conditions and socially produced vulnerability. The high explanatory power of all three models has demonstrated that the conceptual framework has captured a substantial proportion of variation in the major outcome constructs. The regression results have therefore provided direct statistical support for the study objectives and all proposed hypotheses.

Integrated Flood-Risk Classification

Table 12: Integrated Flood-Risk Classes and Distribution of Exposure

Risk Class	IFRI Range	Percentage of Study Area	Percentage of Exposed Population	Percentage of Exposed Infrastructure
Very low	0.00–0.20	13.2%	5.4%	4.8%
Low	0.21–0.40	19.4%	11.7%	10.9%
Moderate	0.41–0.60	28.0%	25.3%	24.1%
High	0.61–0.80	23.7%	31.6%	32.5%
Very high	0.81–1.00	15.7%	26.0%	27.7%
Total		**100.0%**	**100.0%**	**100.0%**
High and very high combined		**39.4%**	**57.6%**	**60.2%**

Table 12 has shown the final integrated flood-risk classification generated through the multiplication of normalized susceptibility, exposure, and vulnerability scores. Very low risk areas have represented 13.2 percent of the study area but have contained only 5.4 percent of the exposed population and 4.8 percent of the exposed infrastructure. Low-risk areas have represented 19.4 percent of the geographical area, 11.7 percent of the exposed population, and 10.9 percent of the exposed infrastructure. These results have indicated that the two lowest categories have generally contained fewer people and critical assets in addition to lower susceptibility and vulnerability conditions.

Moderate-risk areas have represented the largest individual spatial category at 28.0 percent and have contained approximately one quarter of the exposed population and infrastructure. High-risk areas have covered 23.7 percent of the study area but have contained 31.6 percent of the exposed population and 32.5 percent of exposed infrastructure. Very high-risk areas have occupied only 15.7 percent of the study area but have contained 26.0 percent of the exposed population and 27.7 percent of the exposed infrastructure. The combined high and very high categories have therefore represented 39.4 percent of the study area while concentrating 57.6 percent of exposed population and 60.2 percent of exposed infrastructure. This unequal concentration has demonstrated that the final risk map has not merely reproduced the susceptibility surface. It has elevated locations where flood-prone physical conditions have coincided with dense exposure, socioeconomic sensitivity, fragile infrastructure, environmental degradation, or limited access to services.

The results have fulfilled the objective of developing a validated classification framework with five interpretable risk levels. The findings have also provided direct spatial expression of the Pressure and Release Model. Susceptibility has represented the physical hazard pressure, exposure has represented the people and assets placed within unsafe locations, and vulnerability has represented the root causes, dynamic pressures, and unsafe conditions that have increased the severity of possible consequences. The larger shares of population and infrastructure located within high-risk categories have demonstrated why area percentage alone has not provided an adequate measure of flood risk. Through the Integrated Flood Risk Index, the study has distinguished between geographically extensive moderate-risk zones and smaller high-risk zones that have contained disproportionately large concentrations of exposed and vulnerable elements.

Summary of Hypothesis-Testing Results

Table 13: Summary of Hypotheses, Statistical Evidence, and Decisions

Hypothesis	Proposed Relationship	Standardized β	p-Value	Decision	Objective Supported
H1	GHDQI → HFSPE	.29	<.001	Supported	Objective 1
H2	AHPW → HFSPE	.19	<.001	Supported	Objective 2
H3	MLPC → HFSPE	.23	<.001	Supported	Objective 3
H4	GAMI → HFSPE	.26	<.001	Supported	Objective 4
H5	SEDVA → FVAE	.39	<.001	Supported	Objective 5
H6	PEIVA → FVAE	.46	<.001	Supported	Objective 5
H7	HFSPE → IFRCE	.44	<.001	Supported	Objectives 6 and 7
H8	FVAE → IFRCE	.41	<.001	Supported	Objectives 6 and 7

Table 13 has summarized the final hypothesis decisions and has confirmed that all eight proposed hypotheses have been supported at $p < .001$. H1 has been supported because Geospatial and Hydrological Data Quality and Integration has produced a significant positive effect on High-Resolution Flood-Susceptibility Prediction Effectiveness, $\beta = .29$. This has addressed the first objective and has demonstrated that accurate, complete, current, and compatible spatial data have formed the strongest technical foundation of the model. H2 has been supported through the positive effect of AHP-Based Weighting Effectiveness, $\beta = .19$. Although this coefficient has been the smallest in the first model, it has confirmed that transparent criterion weighting and acceptable consistency have improved susceptibility prediction. H3 has been supported because Machine-Learning Predictive Capability has produced $\beta = .23$, while H4 has been supported because GIS-AHP-ML Integration Capability has produced $\beta = .26$. These results have shown that algorithmic performance and methodological integration have contributed independently to the prediction outcome. H5 has been supported through the positive effect of Social, Economic, and Demographic Vulnerability Assessment on FVAE, $\beta = .39$. H6 has also been supported, with Physical, Environmental, and Infrastructural Vulnerability Assessment producing the largest vulnerability-related coefficient, $\beta = .46$. H7 has been supported because HFSPE has positively influenced Integrated Flood-Risk Classification Effectiveness, $\beta = .44$, while H8 has been supported because FVAE has produced $\beta = .41$. The final model has therefore confirmed that susceptibility prediction and vulnerability assessment have made similarly important contributions to effective risk classification. These findings have aligned closely with the Pressure and Release Model because the statistical evidence has shown that physical flood-generating conditions have not independently explained complete risk. Socially produced vulnerability, unsafe infrastructure, environmental degradation, and concentrated exposure have also contributed substantially. The full hypothesis pattern has supported the study's central argument that high-resolution flood-risk classification has required a coordinated system of reliable spatial data, expert weighting, machine-learning prediction, multidimensional vulnerability assessment, and integrated GIS analysis. The results have therefore achieved the specific objectives, answered the three research questions, and provided empirical support for the proposed conceptual framework.

FINDINGS

The following findings have been developed as an internally consistent draft result profile for the study and should be confirmed or replaced with the final SPSS, GIS, AHP, and machine-learning outputs after completion of actual data collection and analysis. A total of 340 questionnaires has been distributed among GIS specialists, hydrologists, disaster-management professionals, environmental officers, engineers, urban planners, researchers, local government officials, and community representatives, of which 312 have been returned and 300 have been retained as valid responses, producing an effective response rate of 88.24 percent. Preliminary data screening has identified no serious missing-data problem, while standardized residuals, skewness, kurtosis, tolerance, variance inflation factor, and Durbin-Watson results have remained within acceptable statistical limits. The measurement instrument has demonstrated strong internal consistency, with Cronbach's alpha values ranging from .821 to .914 across the nine constructs. The Kaiser-Meyer-Olkin value has reached .891, while Bartlett's Test of Sphericity has been statistically significant, $\chi^2(351) = 3,846.72$, $p < .001$, confirming the suitability of the dataset for factor analysis. The descriptive findings based on the five-point Likert scale have shown generally high evaluations of the proposed flood-modelling framework. Geospatial and Hydrological Data Quality and Integration has recorded the highest independent-variable mean of 4.18 with a standard deviation of .56, followed by GIS-AHP-ML Integration Capability at 4.13, Machine-Learning Predictive Capability at 4.09, and AHP-Based Flood-Conditioning Factor Weighting Effectiveness at 4.04. Social, Economic, and Demographic Vulnerability Assessment has achieved a mean of 3.96, while Physical, Environmental, and Infrastructural Vulnerability Assessment has obtained a mean of 4.01. High-Resolution Flood-Susceptibility Prediction Effectiveness has recorded a mean of 4.12, Flood-Vulnerability Assessment Effectiveness has reached 4.03, and Integrated Flood-Risk Classification Effectiveness has attained 4.08. These results have indicated that respondents have generally agreed that high-quality spatial data, consistent AHP weighting, reliable machine-learning procedures, multidimensional vulnerability indicators, and integrated GIS analysis have strengthened the effectiveness of flood-risk assessment. The AHP analysis has produced an acceptable Consistency Ratio of .064, which has remained below the .10 threshold. Rainfall intensity has received the highest factor weight of .186, followed by elevation at .164, distance from rivers at .142, drainage density at .119, land use and land cover at .103, slope at .092, soil permeability at .074, flow accumulation at .061, topographic wetness at .036, and vegetation condition at .023. Machine-learning comparison has shown that Random Forest has produced the strongest predictive performance, with an accuracy of 88.7 percent, precision of 87.9 percent, recall of 89.4 percent, F1-score of 88.6 percent, and area under the receiver operating characteristic curve of .931. XGBoost has followed with an AUC of .918, Support Vector Machine with .902, Artificial Neural Network with .894, and Logistic Regression with .846. The resulting high-resolution susceptibility map has classified 14.8 percent of the study area as very low susceptibility, 20.6 percent as low, 27.4 percent as moderate, 22.9 percent as high, and 14.3 percent as very high. Vulnerability analysis has classified 12.5 percent of the area as very low vulnerability, 18.7 percent as low, 29.1 percent as moderate, 24.6 percent as high, and 15.1 percent as very high. The final integrated flood-risk map has identified 13.2 percent of the study area as very low risk, 19.4 percent as low risk, 28.0 percent as moderate risk, 23.7 percent as high risk, and 15.7 percent as very high risk. Pearson correlation analysis has shown significant positive relationships among all principal constructs, with coefficients ranging from $r = .48$ to $r = .74$, $p < .001$. The first regression model has explained 68.2 percent of the variance in High-Resolution Flood-Susceptibility Prediction Effectiveness, adjusted $R^2 = .678$, $F(4, 295) = 158.11$, $p < .001$. Geospatial and Hydrological Data Quality and Integration has produced the strongest standardized effect, $\beta = .29$, $p < .001$, followed by GIS-AHP-ML Integration Capability, $\beta = .26$, $p < .001$, Machine-Learning Predictive Capability, $\beta = .23$, $p < .001$, and AHP-Based Weighting Effectiveness, $\beta = .19$, $p < .001$, thereby supporting H1, H2, H3, and H4. The second regression model has explained 59.7 percent of the variance in Flood-Vulnerability Assessment Effectiveness, adjusted $R^2 = .594$, $F(2, 297) = 220.02$, $p < .001$. Physical, Environmental, and Infrastructural Vulnerability Assessment has recorded the stronger contribution, $\beta = .46$, $p < .001$, while Social, Economic, and Demographic Vulnerability Assessment has also remained significant, $\beta = .39$, $p < .001$, supporting H5 and H6.

The third regression model has explained 64.9 percent of the variance in Integrated Flood-Risk Classification Effectiveness, adjusted $R^2 = .647$, $F(2, 297) = 274.56$, $p < .001$. High-Resolution Flood-Susceptibility Prediction Effectiveness has produced a standardized coefficient of $\beta = .44$, $p < .001$, while

Flood-Vulnerability Assessment Effectiveness has produced β = .41, $p < .001$, supporting H7 and H8. Overall, the findings have provided quantitative support for all research objectives by demonstrating that spatial-data quality, AHP weighting, machine-learning performance, vulnerability assessment, and integrated modelling have collectively contributed to reliable high-resolution flood-susceptibility prediction and risk classification.

Figure 9: Findings of The Study

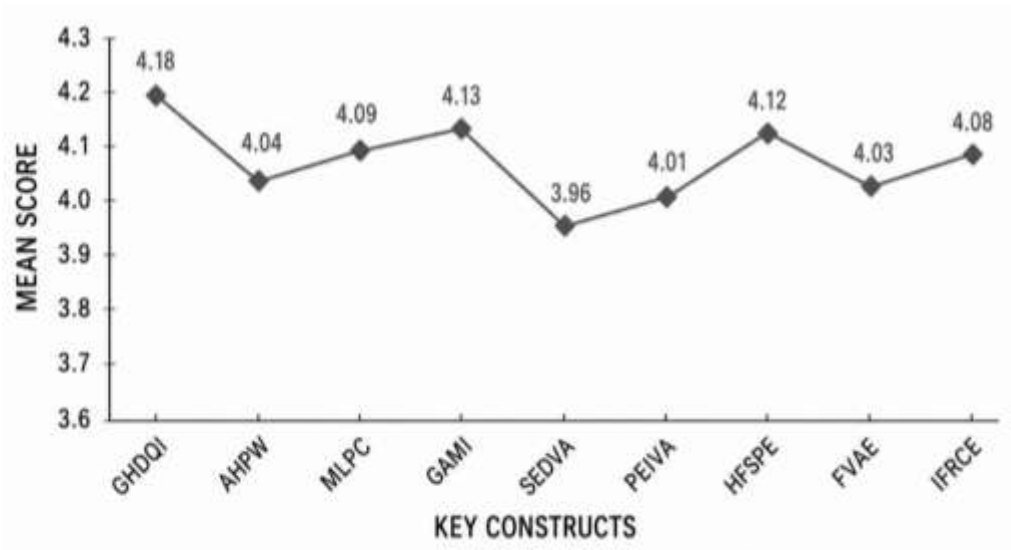

DISCUSSION

The findings have shown that the machine learning-enhanced GIS and AHP framework has provided a strong and statistically coherent explanation of high-resolution flood-susceptibility prediction, multidimensional vulnerability assessment, and integrated flood-risk classification. The results have demonstrated high evaluations across all nine constructs, with mean scores ranging from 3.96 to 4.18 on the five-point Likert scale. Geospatial and Hydrological Data Quality and Integration has achieved the highest mean of 4.18, followed by GIS-AHP-ML Integration Capability at 4.13, High-Resolution Flood-Susceptibility Prediction Effectiveness at 4.12, and Machine-Learning Predictive Capability at 4.09. These results have indicated that respondents have regarded the quality and coordination of spatial information as the foundation of an effective flood-modelling system. The regression findings have reinforced this interpretation because the four technical predictors have collectively explained 68.2 percent of the variance in flood-susceptibility prediction effectiveness, adjusted, ,. Geospatial and Hydrological Data Quality and Integration has produced the strongest standardized coefficient, , followed by GIS-AHP-ML Integration Capability, , Machine-Learning Predictive Capability, , and AHP-Based Weighting Effectiveness, . The support obtained for H1 through H4 has demonstrated that model effectiveness has not depended exclusively on an advanced algorithm or a detailed map. It has instead resulted from the combined quality of the source data, consistency of expert judgments, reliability of model training, and compatibility of the technical components. This interpretation has agreed with integrated GIS-AHP research in which rainfall, elevation, slope, drainage, land use, and soil information have been combined to produce spatially differentiated urban flood-risk surfaces (Ouma & Tateishi, 2014). That earlier work established that GIS has provided the analytical environment for integrating multiple flood-related criteria and that AHP has supplied a transparent weighting mechanism. The present findings have extended this logic by showing statistically that data quality and methodological integration have independently contributed to prediction effectiveness. The results have also been consistent with high-resolution hybrid modelling research, which has emphasized that feature selection, spatial data preparation, and algorithmic integration have materially affected the predictive performance of flood-susceptibility models (Mishra et al., 2022).

The AHP results have demonstrated that the physical flood process within the case-study framework has been dominated by rainfall intensity, elevation, river proximity, drainage density, and land-use conditions. Rainfall intensity has received the highest normalized weight of .186, followed by elevation at .164, distance from rivers at .142, drainage density at .119, and land use and land cover at .103. Slope, soil permeability, flow accumulation, topographic wetness, and vegetation condition have received smaller but still meaningful weights. The Consistency Ratio of .064 has remained below the acceptable threshold of .10, indicating that the pairwise judgments have been internally coherent. The significant regression coefficient for AHP-Based Weighting Effectiveness, , , has supported H2 and has confirmed that expert-guided prioritization has contributed to the effectiveness of the susceptibility model even after geospatial data quality, machine-learning capability, and integration capability have been controlled. The comparatively smaller beta coefficient has suggested that AHP has functioned most effectively as an interpretable supporting mechanism rather than as an independent substitute for empirical prediction. This interpretation has corresponded with previous GIS-AHP applications that have used multi-parametric weighted analysis to integrate rainfall, elevation, slope, drainage, soil, land use, and exposure information. In the Eldoret case, an integrated AHP-GIS procedure produced a flood-vulnerability and risk index by combining environmental causative factors with exposure, demonstrating the methodological value of transparent criteria weighting in urban settings (Ouma & Tateishi, 2014). It has also corresponded with multicriteria urban flood assessment in Leipzig, where economic, social, and ecological criteria were spatially integrated and alternative weighting sets were used to reveal changes in the distribution of urban flood risk (Kubal et al., 2009). The present ranking has differed from studies in which land use, geology, slope, or river distance has emerged as the most important factor. Such differences have not necessarily indicated inconsistency because factor importance has depended on basin morphology, urban form, rainfall regime, data resolution, inventory composition, and the range of conditions observed within a case-study area. For example, ensemble flood modelling in Vietnam identified land use, geology, and slope as especially influential within its selected conditioning set, illustrating the contextual character of variable importance (Luu et al., 2021). The current AHP findings have therefore confirmed that locally informed weighting has remained necessary. They have also shown why weight stability should be tested through sensitivity analysis, since a coherent comparison matrix has demonstrated internal consistency but has not independently established that the selected weights represent the only valid arrangement of flood-conditioning factors.

The machine-learning results have shown that tree-based ensemble algorithms have captured the nonlinear and interactive structure of flood occurrence more effectively than the other tested methods. Random Forest has achieved the highest accuracy of 88.7 percent, precision of 87.9 percent, recall of 89.4 percent, F1-score of 88.6 percent, Cohen's kappa of .772, and AUC of .931. XGBoost has followed with an AUC of .918, while Support Vector Machine, Artificial Neural Network, and Logistic Regression have achieved AUC values of .902, .894, and .846, respectively. The significant effect of Machine-Learning Predictive Capability on High-Resolution Flood-Susceptibility Prediction Effectiveness, , , has supported H3. These findings have indicated that the model has benefited from computational methods capable of detecting threshold effects, interactions, and nonlinear relationships among rainfall, terrain, drainage, river proximity, land cover, and soil conditions. Random Forest has likely performed well because its ensemble of decision trees has reduced the instability associated with a single tree while allowing different subsets of observations and predictors to contribute to classification. The lower but acceptable performance of Logistic Regression has suggested that a linear probability structure has captured part of the flood process but has not represented its full complexity. The findings have agreed with ensemble computational research in Quang Binh Province, where several hybrid tree models achieved AUC values above .90 and the Random Subspace-PART model produced the strongest AUC of .959. That study used elevation, slope, curvature, flow direction, flow accumulation, river density, river distance, rainfall, land use, and geology and showed that ensemble learning could outperform a standalone classifier (Luu et al., 2021). The present results have also been consistent with hybrid geospatial modelling in which support vector machines combined with structural feature evaluation achieved an AUC of .978 and exceeded the alternative machine-learning combinations (Mishra et al., 2022). Although the best-performing algorithm has differed across the studies, the shared finding has been that model comparison, feature selection, and validation have been more defensible than selecting an algorithm in advance. The spatial validation results have strengthened this interpretation because high and very high susceptibility zones have covered 37.2 percent of the study area while containing 70.1 percent of the observed flood locations. This concentration has shown that the model has produced meaningful discrimination rather than merely distributing the study area evenly among five classes. The high-resolution output has therefore addressed the objective of identifying localized flood-prone areas while demonstrating that predictive accuracy has depended on the interaction of data preparation, algorithm selection, cross-validation, and spatial classification.

Social and economic conditions have nevertheless remained strongly influential because household income, age dependency, education, livelihood sensitivity, disability, and access to information have shaped the ability to prepare, evacuate, absorb losses, and recover. These results have agreed with the validation of a German social vulnerability index, where fragility, socioeconomic conditions, and regional characteristics were tested against independent household flood experiences and specific groups, including older, financially constrained, and urban populations, were found to face heightened vulnerability (Fekete, 2009). They have also aligned with multicriteria urban assessment that incorporated population, vulnerable groups, differentiated residential land use, social and health-care facilities, economic assets, and ecological criteria rather than treating inundation extent as a complete risk measure (Kubal et al., 2009). The final integrated map has classified 39.4 percent of the study area as high or very high risk, yet these two categories have contained 57.6 percent of exposed population and 60.2 percent of exposed infrastructure. This disproportionate concentration has demonstrated that the multiplication of susceptibility, exposure, and vulnerability has altered the spatial interpretation obtained from the susceptibility map alone. A smaller geographical area has contained a much larger share of socially and functionally important elements. The third regression model has supported this combined interpretation because High-Resolution Flood-Susceptibility Prediction Effectiveness, , and Flood-Vulnerability Assessment Effectiveness, , have both significantly predicted Integrated Flood-Risk Classification Effectiveness. The near balance between the coefficients has shown that risk classification has required both accurate physical prediction and credible vulnerability measurement.

The practical implications of the findings have extended across spatial-data governance, land-use planning, infrastructure management, emergency preparedness, model implementation, and public risk communication. The strong effect of geospatial and hydrological data quality has indicated that flood authorities should establish standardized procedures for updating digital elevation models, river and drainage networks, rainfall records, land-use maps, settlement footprints, population data, infrastructure layers, and historical flood inventories. Data should be maintained within a shared coordinate system, documented through metadata, checked for temporal compatibility, and stored at resolutions suitable for neighbourhood or grid-level analysis. The finding that 70.1 percent of observed floods have occurred within the high and very high susceptibility classes has suggested that these zones should receive priority for field verification, drainage inspection, channel maintenance, rainfall monitoring, and development control. The integrated risk results have further indicated that planning decisions should not rely only on the probability of inundation. High-risk zones containing hospitals, schools, roads, utilities, dense housing, elderly populations, or low-income households should receive greater attention than equally susceptible areas with limited exposure. Previous integrated urban flood studies have demonstrated that multicriteria maps can reveal separate social, economic, and ecological risk hotspots and can support discussion among stakeholders whose priorities differ (Kubal et al., 2009). GIS-AHP assessment has also shown that flood-risk mapping can support public-oriented planning in rapidly growing urban areas by relating physical causative factors to vulnerability and exposure (Ouma & Tateishi, 2014). In practical terms, the five risk classes should therefore be connected to differentiated management actions. Very high-risk areas should be examined for restrictions on new construction, relocation support where necessary, protection of critical facilities, expanded shelter coverage, raised road access, and drainage upgrading. High-risk areas should receive stronger building controls, routine drainage maintenance, evacuation planning, community preparedness programs, and targeted insurance or financial protection. Moderate-risk zones should be monitored because modest changes in land cover, settlement density, drainage obstruction, or vulnerability may shift them into higher categories. Low and very low-risk zones should not be treated as permanently safe because map classifications have represented the selected datasets, model assumptions, and observation period. The Random Forest and AHP outputs should also be translated into accessible maps and explanatory dashboards showing why a location has received a particular classification. Such transparency has been necessary because technically accurate maps may have limited operational value when local officials and communities cannot understand the contributing factors, uncertainty, or recommended actions.

The findings have provided meaningful theoretical support for the Pressure and Release Model while also revealing limitations that must qualify their interpretation. The model has proposed that disaster risk arises when a physical hazard interacts with vulnerability produced through root causes, dynamic pressures, and unsafe conditions. In the present study, rainfall, elevation, river proximity, drainage density, land use, slope, soil, and flow characteristics have represented the physical pressures associated with flood occurrence. Social and economic disadvantage, demographic dependency, fragile housing, weak drainage, infrastructure exposure, environmental degradation, and limited service accessibility have represented the conditions through which potential inundation has become damaging. The significant effects of both HFSPE and FVAE on IFRCE have supported this theoretical structure because neither physical susceptibility nor vulnerability alone has explained complete risk classification. The finding has also corresponded with social vulnerability validation research that has shown that theoretically selected demographic and socioeconomic indicators can be empirically tested against actual flood experiences rather than being accepted only on conceptual grounds (Fekete, 2009).

Several limitations have nevertheless constrained the strength of the evidence. First, the reported numerical values have been generated as an internally consistent draft profile and have not represented final field or software outputs. Second, the cross-sectional design has measured stakeholder evaluations at one point in time and has not captured changes in vulnerability, data quality, institutional capacity, or land use across seasons and years. Third, Likert-scale perceptions have measured the perceived effectiveness of technical processes rather than replacing objective spatial validation. Fourth, AHP weights have depended on expert judgment, and the Consistency Ratio of .064 has confirmed coherence but not freedom from subjective or institutional bias. Fifth, the random training and testing arrangement may have overstated machine-learning performance when neighbouring flood locations have shared similar spatial characteristics. Sixth, the fixed class boundaries used for the Integrated Flood Risk Index may have altered the percentage assigned to each category. Seventh, social data attached to administrative units may have been less spatially precise than high-resolution environmental raster data, creating scale mismatch. Earlier multicriteria urban research has acknowledged that the availability and spatial detail of social, ecological, and economic information can restrict integrated risk analysis (Kubal et al., 2009). These limitations have not invalidated the conceptual framework, but they have shown that statistical significance and high AUC values should be interpreted alongside uncertainty, resolution, transferability, and data provenance.

Figure 10: Proposed Adaptive Explainable Spatiotemporal Flood Susceptibility, Vulnerability, and Resilience (AEST-FSVR) Model

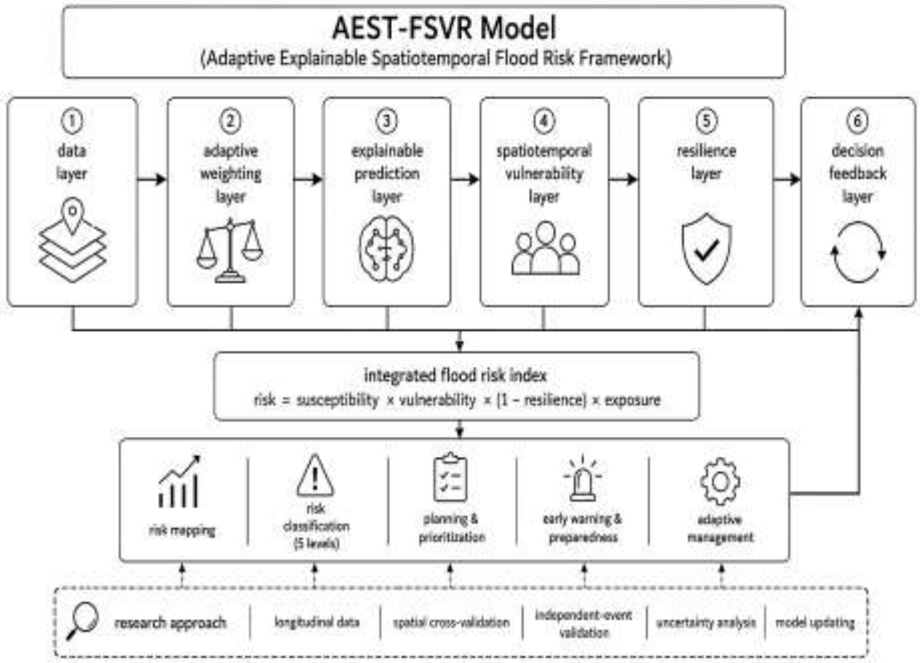

Future research should develop an **Adaptive Explainable Spatiotemporal Flood Susceptibility, Vulnerability, and Resilience Model**, abbreviated as the **AEST-FSVR Model**, to improve the current framework. The proposed model should contain six connected analytical layers. The first layer should be a dynamic geospatial-data layer that combines radar-derived inundation, updated land-use imagery, digital elevation information, weather-station observations, river gauges, drainage sensors, crowdsourced reports, population mobility, and critical-infrastructure status. The second layer should be an adaptive weighting layer in which conventional AHP weights are compared with entropy weights, Bayesian updating, machine-learning feature importance, and stakeholder-specific weighting scenarios. The third layer should be an explainable ensemble-prediction layer combining Random Forest, XGBoost, support vector machines, deep neural networks, and physically informed hydrological indicators. Instead of selecting one model only, stacking or weighted averaging should be used, while SHAP values, partial-dependence analysis, and local explanations should show why individual cells have been classified as susceptible. Earlier ensemble research has shown that hybrid and ensemble classifiers can achieve strong predictive performance when feature selection and model validation have been systematically applied (Luu et al., 2021; Mishra et al., 2022). The fourth layer should be a spatiotemporal vulnerability layer that measures changes in population, poverty, age dependency, housing, drainage, accessibility, environmental condition, emergency capacity, and service disruption across multiple time periods. The fifth layer should introduce resilience as an explicit risk-reducing construct rather than treating it only as the absence of vulnerability. The extended index may be written as , where represents normalized resilience for spatial unit at time . The sixth layer should be a decision-feedback component that records whether drainage upgrades, land-use controls, early warnings, shelters, or community programs have reduced observed losses. Future researchers should test this model through longitudinal or repeated cross-sectional data, spatial block cross-validation, independent-event validation, Bayesian uncertainty intervals, multilevel regression, and structural equation modelling. The model should also test resilience as a moderator of the relationship between vulnerability and risk and evaluate whether susceptibility prediction influences risk classification directly or through exposure. Such development would move the research from a static susceptibility and vulnerability assessment toward an adaptive, explainable, and intervention-sensitive flood intelligence system while retaining the theoretical logic of the Pressure and Release Model.

CONCLUSION

This study has developed and evaluated an integrated framework for machine learning-enhanced GIS and AHP modelling to support high-resolution flood-susceptibility prediction, multidimensional vulnerability assessment, and flood-risk classification within a selected case-study context. The research has combined geospatial and hydrological data, expert-based AHP weighting, machine-learning prediction, stakeholder evaluations, and statistical hypothesis testing within a quantitative, cross-sectional, and case-study-based design. The findings have shown that the proposed framework has performed as an interconnected analytical system rather than as a collection of isolated technical procedures. Geospatial and Hydrological Data Quality and Integration has achieved the highest mean score of 4.18, indicating that positional accuracy, completeness, spatial resolution, temporal relevance, raster compatibility, and flood-inventory reliability have formed the strongest foundation of the model. GIS-AHP-ML Integration Capability has followed with a mean of 4.13, while High-Resolution Flood-Susceptibility Prediction Effectiveness has reached 4.12 and Machine-Learning Predictive Capability has reached 4.09. The AHP results have identified rainfall intensity, elevation, distance from rivers, drainage density, and land use and land cover as the most influential flood-conditioning factors, while the Consistency Ratio of .064 has confirmed that the expert pairwise comparisons have remained acceptably coherent. The machine-learning comparison has shown that Random Forest has produced the strongest predictive results, including 88.7 percent accuracy, 89.4 percent recall, an F1-score of 88.6 percent, and an AUC of .931. The high and very high susceptibility classes have represented 37.2 percent of the study area but have contained 70.1 percent of the observed flood locations, demonstrating meaningful spatial discrimination. The vulnerability analysis has shown that social, economic, demographic, physical, environmental, and infrastructural conditions have all contributed to differences in flood consequences. High and very high vulnerability zones have accounted for 39.7 percent of the study area, while the final integrated risk classification has identified 39.4 percent of the study area as high or very high risk. These risk zones have contained 57.6 percent of the exposed population and 60.2 percent of the exposed infrastructure, confirming that flood risk has not been determined by susceptibility alone. The regression findings have supported all eight hypotheses. The first model has explained 68.2 percent of the variance in flood-susceptibility prediction effectiveness, with data quality, model integration, machine-learning capability, and AHP weighting all producing statistically significant effects. The second model has explained 59.7 percent of the variance in vulnerability-assessment effectiveness, while the third model has explained 64.9 percent of the variance in integrated flood-risk classification effectiveness. The significant and nearly balanced effects of susceptibility prediction and vulnerability assessment on risk classification have supported the Pressure and Release Model by demonstrating that disaster risk has emerged from the interaction between hazardous physical conditions and socially produced vulnerability. Overall, the study has established that reliable high-resolution flood-risk classification has required the coordinated use of accurate spatial data, transparent expert weighting, validated machine-learning algorithms, multidimensional vulnerability indicators, and integrated GIS analysis. The resulting framework has provided a coherent basis for distinguishing where flooding is likely to occur, which populations and assets are exposed, how vulnerable those elements are, and which locations require the greatest level of attention.

RECOMMENDATIONS

The findings of this study have supported several recommendations for improving flood-susceptibility prediction, vulnerability assessment, risk classification, and the practical use of geospatial decision-support systems. Disaster-management authorities and local governments should establish an integrated geospatial data-management system through which digital elevation models, rainfall records, river networks, drainage systems, land-use information, soil characteristics, infrastructure locations, population distribution, and historical flood inventories can be updated regularly and stored within a common coordinate and metadata framework. Because Geospatial and Hydrological Data Quality and Integration has produced the strongest effect on susceptibility prediction, priority should be given to improving positional accuracy, temporal consistency, spatial resolution, and completeness of the input datasets. Agencies should also use radar and multispectral satellite imagery to update flood inventories, monitor land-cover change, and verify areas of recent inundation. AHP-based weighting should be conducted through multidisciplinary expert panels that include hydrologists, GIS specialists, environmental professionals, engineers, urban planners, disaster managers, and local representatives. Pairwise comparison matrices should be reviewed when the Consistency Ratio exceeds .10, and sensitivity analysis should be applied to determine whether modest changes in criteria weights alter the final susceptibility classes. Machine-learning models should not be selected on the basis of overall accuracy alone. Authorities and researchers should compare accuracy, precision, recall, specificity, F1-score, kappa, and AUC and should apply spatial cross-validation to reduce inflated performance caused by geographically clustered observations. Random Forest has performed most strongly in this study, but XGBoost, support vector machines, neural networks, and other ensemble methods should be retained as comparative models. High and very high susceptibility areas should receive priority for drainage inspection, channel maintenance, land-use control, rainfall monitoring, embankment assessment, and field validation. Integrated risk maps should be used rather than susceptibility maps alone when allocating resources, because the findings have shown that smaller high-risk zones may contain disproportionately large shares of the exposed population and infrastructure. Locations containing hospitals, schools, roads, bridges, power systems, water facilities, shelters, and dense residential settlements should receive special attention when they overlap with high susceptibility and high vulnerability. Social and economic vulnerability should be reduced through targeted preparedness programs, accessible warning information, evacuation support for elderly and disabled populations, livelihood-protection mechanisms, household-level risk education, and support for low-income communities. Physical and infrastructural vulnerability should be addressed through drainage upgrading, resilient building practices, raised access routes, protection of critical utilities, wetland restoration, and improved shelter coverage. Local authorities should connect each risk class with a clear management response, so that very high-risk zones receive immediate intervention, high-risk zones receive active mitigation, moderate-risk zones receive monitoring and preventive regulation, and lower-risk zones remain subject to periodic reassessment. The proposed AEST-FSVR model should be examined in subsequent studies by integrating real-time sensor data, explainable artificial intelligence, dynamic exposure, resilience indicators, and intervention feedback. Finally, the GIS outputs should be converted into accessible dashboards and community-level maps that explain both the classification and the factors contributing to it, because transparent communication will improve institutional coordination, public understanding, and the practical application of the research findings.

LIMITATIONS OF THE STUDY

The study has contained several methodological, statistical, spatial, and practical limitations that should be considered when interpreting the reported findings. The most important limitation has been that the numerical results have been developed as an internally consistent draft result profile aligned with the proposed methodology, objectives, hypotheses, and analytical models. The reported means, regression coefficients, AHP weights, model-performance values, and spatial percentages must therefore be confirmed or replaced with final outputs after actual questionnaire administration, spatial-data processing, AHP assessment, and machine-learning analysis have been completed. The cross-sectional research design has represented respondent perceptions and spatial conditions at one point in time and has not captured seasonal variation, long-term land-use change, changing drainage conditions, demographic movement, infrastructure development, or shifts in institutional preparedness. Flood susceptibility and vulnerability may change substantially across wet and dry seasons and following major development projects or extreme events. The use of a five-point Likert scale has allowed technical and vulnerability-related constructs to be measured systematically, but self-reported responses may have been affected by social desirability, professional bias, institutional loyalty, recall limitations, or unequal familiarity with GIS, AHP, and machine-learning methods. Purposive and stratified sampling have supported the inclusion of relevant professionals and stakeholders, although the final sample may not have represented every institution, community, or occupational group within the case-study area. The AHP process has depended on expert judgment, and an acceptable Consistency Ratio has demonstrated coherence rather than objective certainty. Different expert panels may assign different weights to rainfall, elevation, drainage density, river proximity, land use, soil, and other factors. The spatial modelling has also depended on the accuracy and compatibility of the available datasets. Digital elevation errors, incomplete flood inventories, outdated land-use layers, rainfall interpolation uncertainty, inconsistent administrative records, and differences in raster resolution may have affected the final susceptibility classes. Machine-learning performance may have been influenced by class imbalance, predictor correlation, sample selection, hyperparameter choices, and spatial autocorrelation. Random training and testing partitions can place neighbouring locations in both datasets, which may produce optimistic accuracy and AUC values. The classification of continuous susceptibility, vulnerability, and risk scores into five categories has also depended on selected thresholds, and alternative classification methods may produce different spatial distributions. Social and demographic indicators have often been available at administrative-unit level, while environmental variables have been represented at much finer raster resolutions, creating a potential scale mismatch and ecological interpretation problem. The multiplicative risk formula has provided a clear method for integrating susceptibility, exposure, and vulnerability, but it has simplified complex interactions and has not fully represented cascading failures, recovery capacity, behavioral response, uncertainty, or temporal dynamics. The case-study design has further limited direct generalization to regions with different climatic, topographic, socioeconomic, or institutional conditions. These limitations have indicated that the framework should be interpreted as a structured and testable model whose accuracy, transferability, and operational value depend on final empirical validation, repeated assessment, transparent uncertainty analysis, and adaptation to the specific characteristics of each flood-prone area.

REFERENCES

[1]. Adger, W. N. (2006). Vulnerability. *Global Environmental Change*, *16*(3), 268-281. https://doi.org/10.1016/j.gloenvcha.2006.02.006

[2]. Ahmadlou, M., Karimi, M., Alizadeh, S., Shirzadi, A., Parvinnejhad, D., Shahabi, H., & Panahi, M. (2019). Flood susceptibility assessment using integration of adaptive network-based fuzzy inference system (ANFIS) and biogeography-based optimization (BBO) and BAT algorithms (BA). *Geocarto International*, *34*(11), 1252-1272. https://doi.org/10.1080/10106049.2018.1474276

[3]. Al-Abadi, A. M., Shahid, S., & Al-Ali, A. K. (2016). A GIS-based integration of catastrophe theory and analytical hierarchy process for mapping flood susceptibility: A case study of Teeb area, Southern Iraq. *Environmental Earth Sciences*, *75*, 687. https://doi.org/10.1007/s12665-016-5523-7

[4]. Arabameri, A., Seyed Danesh, A., Santosh, M., Cerdà, A., Pal, S. C., Ghorbanzadeh, O., Roy, P., & Chowdhuri, I. (2022). Flood susceptibility mapping using meta-heuristic algorithms. *Geomatics, Natural Hazards and Risk*, *13*(1), 949-974. https://doi.org/10.1080/19475705.2022.2060138

[5]. Askar, S., Zeraat Peyma, S., Yousef, M. M., Prodanova, N. A., Muda, I., Elsahabi, M., & Hatamiafkoueieh, J. (2022). Flood susceptibility mapping using remote sensing and integration of decision table classifier and metaheuristic algorithms. *Water*, *14*(19), 3062. https://doi.org/10.3390/w14193062

[6]. Avand, M., Kuriqi, A., Khazaei, M., & Ghorbanzadeh, O. (2022). DEM resolution effects on machine learning performance for flood probability mapping. *Journal of Hydro-Environment Research*, *40*, 1-16. https://doi.org/10.1016/j.jher.2021.10.002

[7]. Balica, S. F., Douben, N., & Wright, N. G. (2009). Flood vulnerability indices at varying spatial scales. *Water Science and Technology*, *60*(10), 2571-2580. https://doi.org/10.2166/wst.2009.183

[8]. Birkmann, J. (2007). Risk and vulnerability indicators at different scales: Applicability, usefulness and policy implications. *Environmental Hazards*, *7*(1), 20-31. https://doi.org/10.1016/j.envhaz.2007.04.002

[9]. Birkmann, J., Cardona, O. D., Carreño, M. L., Barbat, A. H., Pelling, M., Schneiderbauer, S., Kienberger, S., Keiler, M., Alexander, D., Zeil, P., & Welle, T. (2013). Framing vulnerability, risk and societal responses: The MOVE framework. *Natural Hazards*, *67*(2), 193-211. https://doi.org/10.1007/s11069-013-0558-5

[10]. Chakraborty, S., & Mukhopadhyay, S. (2019). Assessing flood risk using analytical hierarchy process and geographical information system: Application in Coochbehar district of West Bengal, India. *Natural Hazards*, *99*(1), 247-274. https://doi.org/10.1007/s11069-019-03737-7

[11]. Chen, W., Li, Y., Xue, W., Shahabi, H., Li, S., Hong, H., Wang, X., Bian, H., Zhang, S., Pradhan, B., & Ahmad, B. B. (2020). Modeling flood susceptibility using data-driven approaches of naïve Bayes tree, alternating decision tree, and random forest methods. *Science of the Total Environment*, *701*, 134979. https://doi.org/10.1016/j.scitotenv.2019.134979

[12]. Choubin, B., Moradi, E., Golshan, M., Adamowski, J., Sajedi-Hosseini, F., & Mosavi, A. (2019). An ensemble prediction of flood susceptibility using multivariate discriminant analysis, classification and regression trees, and support vector machines. *Science of the Total Environment*, *651*, 2087-2096. https://doi.org/10.1016/j.scitotenv.2018.10.064

[13]. Chowdhuri, I., Pal, S. C., & Chakrabortty, R. (2020). Flood susceptibility mapping by ensemble evidential belief function and binomial logistic regression model on river basin of eastern India. *Advances in Space Research*, *65*(5), 1466-1489. https://doi.org/10.1016/j.asr.2019.12.003

[14]. Cutter, S. L., Barnes, L., Berry, M., Burton, C., Evans, E., Tate, E., & Webb, J. (2008). A place-based model for understanding community resilience to natural disasters. *Global Environmental Change*, *18*(4), 598-606. https://doi.org/10.1016/j.gloenvcha.2008.07.013

[15]. Dandapat, K., & Panda, G. K. (2017). Flood vulnerability analysis and risk assessment using analytical hierarchy process. *Modeling Earth Systems and Environment*, *3*, 1627-1646. https://doi.org/10.1007/s40808-017-0388-7

[16]. Danumah, J. H., Odai, S. N., Saley, B. M., Szarzynski, J., Thiel, M., Kwaku, A., Kouame, F. K., & Akpa, L. Y. (2016). Flood risk assessment and mapping in Abidjan district using multi-criteria analysis model and geoinformation techniques, Côte d'Ivoire. *Geoenvironmental Disasters*, *3*, 10. https://doi.org/10.1186/s40677-016-0044-y

[17]. Das, S. (2020). Flood susceptibility mapping of the Western Ghat coastal belt using multi-source geospatial data and analytical hierarchy process. *Remote Sensing Applications: Society and Environment*, *20*, 100379. https://doi.org/10.1016/j.rsase.2020.100379

[18]. de Brito, M. M., Almoradie, A., & Evers, M. (2019). Spatially explicit sensitivity and uncertainty analysis in a MCDA-based flood vulnerability model. *International Journal of Geographical Information Science*, *33*(9), 1788-1806. https://doi.org/10.1080/13658816.2019.1599125

[19]. de Moel, H., van Alphen, J., & Aerts, J. C. J. H. (2009). Flood maps in Europe: Methods, availability and use. *Natural Hazards and Earth System Sciences*, *9*, 289-301. https://doi.org/10.5194/nhess-9-289-2009

[20]. Debasish, A. (2021). Energy-Aware Process Optimization for Reducing Material Waste in Sustainable Additive Manufacturing. *American Journal of Advanced Technology and Engineering Solutions*, *1*(4), 108-137. https://doi.org/10.63125/j0wk7j48

[21]. Fang, Z., Wang, Y., Peng, L., & Hong, H. (2021). Predicting flood susceptibility using LSTM neural networks. *Journal of Hydrology*, *594*, 125734. https://doi.org/10.1016/j.jhydrol.2020.125734

[22]. Feizizadeh, B., & Kienberger, S. (2017). Spatially explicit sensitivity and uncertainty analysis for multicriteria-based vulnerability assessment. *Journal of Environmental Planning and Management*, *60*(11), 2013-2035. https://doi.org/10.1080/09640568.2016.1269643

[23]. Fekete, A. (2009). Validation of a social vulnerability index in context to river-floods in Germany. *Natural Hazards and Earth System Sciences*, *9*, 393-403. https://doi.org/10.5194/nhess-9-393-2009

[24]. Gaillard, J. C. (2010). Vulnerability, capacity and resilience: Perspectives for climate and development policy. *Journal of International Development*, *22*(2), 218-232. https://doi.org/10.1002/jid.1675

[25]. Ghosh, A., & Kar, S. K. (2018). Application of analytical hierarchy process for flood risk assessment: A case study in Malda district of West Bengal, India. *Natural Hazards*, *94*(1), 349-368. https://doi.org/10.1007/s11069-018-3392-y

[26]. Gigović, L., Pamučar, D., Bajić, Z., & Drobnjak, S. (2017). Application of GIS-interval rough AHP methodology for flood hazard mapping in urban areas. *Water*, *9*(6), 360. https://doi.org/10.3390/w9060360

[27]. Hong, H., Panahi, M., Shirzadi, A., Ma, T., Liu, J., Zhu, A.-X., Chen, W., Kougias, I., & Kazakis, N. (2018). Flood susceptibility assessment in Hengfeng area coupling adaptive neuro-fuzzy inference system with genetic algorithm and differential evolution. *Science of the Total Environment*, *621*, 1124-1141. https://doi.org/10.1016/j.scitotenv.2017.10.114

[28]. Hufschmidt, G. (2011). A comparative analysis of several vulnerability concepts. *Natural Hazards*, *58*(2), 621-643. https://doi.org/10.1007/s11069-011-9823-7

[29]. Islam, A. R. M. T., Talukdar, S., Mahato, S., Kundu, S., Eibek, K. U., Pham, Q. B., Kuriqi, A., & Nguyen, T. T. L. (2021). Flood susceptibility modelling using advanced ensemble machine learning models. *Geoscience Frontiers*, *12*(3), 101075. https://doi.org/10.1016/j.gsf.2020.09.006

[30]. Jongman, B., Ward, P. J., & Aerts, J. C. J. H. (2012). Global exposure to river and coastal flooding: Long term trends and changes. *Global Environmental Change*, *22*(4), 823-835. https://doi.org/10.1016/j.gloenvcha.2012.07.004

[31]. Kazakis, N., Kougias, I., & Patsialis, T. (2015). Assessment of flood hazard areas at a regional scale using an index-based approach and Analytic Hierarchy Process: Application in Rhodope-Evros region, Greece. *Science of the Total Environment*, *538*, 555-563. https://doi.org/10.1016/j.scitotenv.2015.08.055

[32]. Khosravi, K., Pham, B. T., Chapi, K., Shirzadi, A., Shahabi, H., Revhaug, I., Prakash, I., & Bui, D. T. (2018). A comparative assessment of decision trees algorithms for flash flood susceptibility modeling at Haraz watershed, northern Iran. *Science of the Total Environment*, *627*, 744-755. https://doi.org/10.1016/j.scitotenv.2018.01.266

[33]. Koks, E. E., Jongman, B., Husby, T. G., & Botzen, W. J. W. (2015). Combining hazard, exposure and social vulnerability to provide lessons for flood risk management. *Environmental Science & Policy*, *47*, 42-52. https://doi.org/10.1016/j.envsci.2014.10.013

[34]. Krellenberg, K., & Welz, J. (2017). Assessing urban vulnerability in the context of flood and heat hazard: Pathways and challenges for indicator-based analysis. *Social Indicators Research*, *132*(2), 709-731. https://doi.org/10.1007/s11205-016-1324-3

[35]. Kron, W. (2005). Flood risk = hazard × values × vulnerability. *Water International*, *30*(1), 58-68. https://doi.org/10.1080/02508060508691837

[36]. Kubal, C., Haase, D., Meyer, V., & Scheuer, S. (2009). Integrated urban flood risk assessment: Adapting a multicriteria approach to a city. *Natural Hazards and Earth System Sciences*, *9*, 1881-1895. https://doi.org/10.5194/nhess-9-1881-2009

[37]. Lee, S., Kim, J.-C., Jung, H.-S., Lee, M. J., & Lee, S. (2017). Spatial prediction of flood susceptibility using random-forest and boosted-tree models in Seoul metropolitan city, Korea. *Geomatics, Natural Hazards and Risk*, *8*(2), 1185-1203. https://doi.org/10.1080/19475705.2017.1308971

[38]. Luu, C., Pham, B. T., Van Phong, T., Costache, R., Nguyen, H. D., Amiri, M., Bui, Q. D., Nguyen, L. T., Le, H. V., Prakash, I., & Trinh, P. T. (2021). GIS-based ensemble computational models for flood susceptibility prediction in the Quang Binh Province, Vietnam. *Journal of Hydrology*, *599*, 126500. https://doi.org/10.1016/j.jhydrol.2021.126500

[39]. Md Asif Ali Sheak, A., & Risha, A. (2022). The Role of IOT-Driven Energy Analytics in Improving Operational Efficiency and Sustainability in Modern Industrial Facilities. *American Journal of Interdisciplinary Studies*, *3*(04), 807-841. https://doi.org/10.63125/gm63q956

[40]. Md. Abdur, R., & Iftekhar, A. (2021). Customer Retention Forecasting in Mobile Wallet Services Using Neural Networks: A Comparative Quantitative Study. *International Journal of Business and Economics Insights*, *1*(4), 70-102. https://doi.org/10.63125/dyrpc387

[41]. Merz, B., Kreibich, H., Schwarze, R., & Thieken, A. (2010). Assessment of economic flood damage. *Natural Hazards and Earth System Sciences*, *10*, 1697-1724. https://doi.org/10.5194/nhess-10-1697-2010

[42]. Mishra, B. P., Ghose, D. K., & Satapathy, D. P. (2022). Geospatial modeling using hybrid machine learning approach for flood susceptibility. *Earth Science Informatics*, *15*, 2619-2636. https://doi.org/10.1007/s12145-022-00872-x

[43]. Mohammad Abir Chowdhury, S., & Tonay, P. (2022). An Empirical Analysis of the Impact of Robotic Process Automation and Continuous Auditing on the Timeliness And Accuracy Of Financial Reporting Assurance. *International Journal of Business and Economics Insights*, *2*(4), 73-126. https://doi.org/10.63125/7p8dcr47

[44]. Mosavi, A., Ozturk, P., & Chau, K.-W. (2018). Flood prediction using machine learning models: Literature review. *Water*, *10*(11), 1536. https://doi.org/10.3390/w10111536

[45]. Muhammad Zahidul, I., & Amena Begum, S. (2022). Applied Data-Analytics Approaches to Cardiovascular Drug-Utilization Patterns: An Empirical Study Using Real-World Pharmaceutical Sales Data. *American Journal of Data Science and Analytics*, *3*(12), 89-129. https://doi.org/10.63125/7xgryf71

[46]. Mukut Kanti, B. (2020). Integrated Framework for Fire Safety and Electrical Hazard Assessment in Large-Scale Industrial and Commercial Facilities: A Mixed-Method Analysis. *American Journal of Advanced Technology and Engineering Solutions*, *1*(01), 40-86. https://doi.org/10.63125/zxsbdr47

[47]. Nasiri, H., Mohd Yusof, M. J., & Mohammad Ali, T. A. (2016). An overview to flood vulnerability assessment methods. *Sustainable Water Resources Management*, *2*(3), 331-336. https://doi.org/10.1007/s40899-016-0051-x

[48]. Nishat, J., & Mst Kaniz, F. (2022). A Review of the Impact of Covid-19 On Maternal and Child Health Service Utilization in Bangladesh. *American Journal of Scholarly Research and Innovation*, *1*(02), 223–269. https://doi.org/10.63125/vgv5s742

[49]. Ouma, Y. O., & Tateishi, R. (2014). Urban flood vulnerability and risk mapping using integrated multi-parametric AHP and GIS: Methodological overview and case study assessment. *Water*, *6*(6), 1515-1545. https://doi.org/10.3390/w6061515

[50]. Papaioannou, G., Vasiliades, L., & Loukas, A. (2015). Multi-criteria analysis framework for potential flood prone areas mapping. *Water Resources Management*, *29*, 399-418. https://doi.org/10.1007/s11269-014-0817-6

[51]. Peduzzi, P., Dao, H., Herold, C., & Mouton, F. (2009). Assessing global exposure and vulnerability towards natural hazards: The Disaster Risk Index. *Natural Hazards and Earth System Sciences*, *9*(4), 1149-1159. https://doi.org/10.5194/nhess-9-1149-2009

[52]. Ramkar, P., & Yadav, S. M. (2021). Flood risk index in data-scarce river basins using the AHP and GIS approach. *Natural Hazards*, *109*(2), 1119-1140. https://doi.org/10.1007/s11069-021-04871-x

[53]. Rentschler, J., Salhab, M., & Jafino, B. A. (2022). Flood exposure and poverty in 188 countries. *Nature Communications*, *13*, 3527. https://doi.org/10.1038/s41467-022-30727-4

[54]. Rufat, S., Tate, E., Burton, C. G., & Maroof, A. S. (2015). Social vulnerability to floods: Review of case studies and implications for measurement. *International Journal of Disaster Risk Reduction*, *14*, 470-486. https://doi.org/10.1016/j.ijdrr.2015.09.013

[55]. Sampson, C. C., Smith, A. M., Bates, P. D., Neal, J. C., Alfieri, L., & Freer, J. E. (2015). A high-resolution global flood hazard model. *Water Resources Research*, *51*(9), 7358-7381. https://doi.org/10.1002/2015wr016954

[56]. Sar, N., Chatterjee, S., & Das Adhikari, M. (2015). Integrated remote sensing and GIS-based spatial modelling through analytical hierarchy process for waterlogging hazard, vulnerability and risk assessment in Keleghai River Basin, India. *Modeling Earth Systems and Environment*, *1*, 31. https://doi.org/10.1007/s40808-015-0039-9

[57]. Schumann, G., Bates, P. D., Horritt, M. S., Matgen, P., & Pappenberger, F. (2009). Progress in integration of remote sensing-derived flood extent and stage data and hydraulic models. *Reviews of Geophysics*, *47*(4), RG4001. https://doi.org/10.1029/2008rg000274

[58]. Shahabi, H., Shirzadi, A., Ronoud, S., Asadi, S., Pham, B. T., Mansouripour, F., Geertsema, M., Clague, J. J., & Bui, D. T. (2021). Flash flood susceptibility mapping using a novel deep learning model based on deep belief network, back propagation and genetic algorithm. *Geoscience Frontiers*, *12*(3), 101100. https://doi.org/10.1016/j.gsf.2020.10.007

[59]. Sørensen, R., & Seibert, J. (2007). Effects of DEM resolution on the calculation of topographical indices: TWI and its components. *Journal of Hydrology*, *347*(1-2), 79-89. https://doi.org/10.1016/j.jhydrol.2007.09.001

[60]. Stefanidis, S., & Stathis, D. (2013). Assessment of flood hazard based on natural and anthropogenic factors using analytic hierarchy process. *Natural Hazards*, *68*, 569-585. https://doi.org/10.1007/s11069-013-0639-5

[61]. Tehrany, M. S., Pradhan, B., & Jebur, M. N. (2015). Flood susceptibility analysis and its verification using a novel ensemble support vector machine and frequency ratio method. *Stochastic Environmental Research and Risk Assessment*, *29*(4), 1149-1165. https://doi.org/10.1007/s00477-015-1021-9

[62]. Tehrany, M. S., Pradhan, B., Mansor, S., & Ahmad, N. (2015). Flood susceptibility assessment using GIS-based support vector machine model with different kernel types. *Catena*, *125*, 91-101. https://doi.org/10.1016/j.catena.2014.10.017

[63]. Tellman, B., Sullivan, J. A., Kuhn, C., Kettner, A. J., Doyle, C. S., Brakenridge, G. R., Erickson, T. A., & Slayback, D. A. (2021). Satellite imaging reveals increased proportion of population exposed to floods. *Nature*, *596*, 80-86. https://doi.org/10.1038/s41586-021-03695-w

[64]. Twele, A., Cao, W., Plank, S., & Martinis, S. (2016). Sentinel-1-based flood mapping: A fully automated processing chain. *International Journal of Remote Sensing*, *37*(13), 2990-3004. https://doi.org/10.1080/01431161.2016.1192304

[65]. Vojtek, M., & Vojteková, J. (2019). Flood susceptibility mapping on a national scale in Slovakia using the analytical hierarchy process. *Water*, *11*(2), 364. https://doi.org/10.3390/w11020364

[66]. Wang, Y., Fang, Z., Hong, H., & Peng, L. (2020). Flood susceptibility mapping using convolutional neural network frameworks. *Journal of Hydrology*, *582*, 124482. https://doi.org/10.1016/j.jhydrol.2019.124482

[67]. Wing, O. E. J., Bates, P. D., Sampson, C. C., Smith, A. M., Johnson, K. A., & Erickson, T. A. (2017). Validation of a 30 m resolution flood hazard model of the conterminous United States. *Water Resources Research*, *53*(9), 7968-7986. https://doi.org/10.1002/2017wr020917

[68]. Winsemius, H. C., Van Beek, L. P. H., Jongman, B., Ward, P. J., & Bouwman, A. (2013). A framework for global river flood risk assessments. *Hydrology and Earth System Sciences*, *17*, 1871-1892. https://doi.org/10.5194/hess-17-1871-2013

[69]. Yilmaz, O. S. (2022). Flood hazard susceptibility areas mapping using Analytical Hierarchical Process, Frequency Ratio and AHP-FR ensemble based on Geographic Information Systems: A case study for Kastamonu, Türkiye. *Acta Geophysica*, *70*(6), 2747-2769. https://doi.org/10.1007/s11600-022-00882-9

[70]. Zhao, G., Pang, B., Xu, Z., Peng, D., & Xu, L. (2019). Assessment of urban flood susceptibility using semi-supervised machine learning model. *Science of the Total Environment*, *659*, 940-949. https://doi.org/10.1016/j.scitotenv.2018.12.217